

# Imaging the Deep Crustal Structure of Central Oklahoma using Stacking and Inversion of Local Earthquake Waveforms

Pranshu Ratre<sup>1,1</sup> and Michael Behm<sup>1,1</sup>

<sup>1</sup>University of Oklahoma

November 30, 2022

## Abstract

The southern Granite-Rhyolite province contains a comprehensive record of lithospheric evolution in North America. During the last decade, increased seismicity along with improved seismic monitoring installations in Oklahoma provided a rich catalog of local earthquakes. The source-receiver geometry of this dataset is well posed to illuminate the middle and lower crust through long offset recordings of the Pg phase. We present a 3-D P-wave velocity model for central and north Oklahoma developed through a non-standard processing scheme applied to local earthquake waveforms recorded from 2010-2017, focusing on the deeper crust. We employed common-mid-point sorting, stacking, and inversion of Pg-phases which resulted in a set of localized velocity-depth functions up to depths of 40 km. Using this methodology, we significantly increased the S/N ratio for far offset (~250 km) local earthquake waveforms which led to the increase in depth of investigation for our final 3-D velocity model. We find high velocity (> 7 km/s) lower crust throughout the investigated area which suggests a mafic lower crust. The high velocities support previously established models which state that the lower crust of the Granite-Rhyolite province was derived from melting of older crust. We further relate shallow and middle crustal velocity anomalies to other data sets such as gravimetric and magnetic anomalies, and the spatial distribution of earthquakes. We interpret the Nemaha Fault system as a deep-rooted discontinuity which separates two crustal domains. On the contrary, we do not find clear evidence for the existence of the Midcontinent rift (MCR) in northern Oklahoma.

# 1 **Imaging the Deep Crustal Structure of Central Oklahoma using** 2 **Stacking and Inversion of Local Earthquake Waveforms**

3 **Pranshu Ratre<sup>1</sup>, Michael Behm<sup>1</sup>**

4 <sup>1</sup>School of Geosciences, University of Oklahoma

## 5 **Key Points:**

- 6 • 3-D Pg wave velocity model for the Southern-Granite Rhyolite province in central  
7 Oklahoma up to depth of 40km.
- 8 • High velocity ( $V_p > 7\text{km/s}$ ) lower crust suggests a mafic lower crust.
- 9 • High velocity anomalies observed in the upper-to-middle crust but lack of clear  
10 evidence for a rift structure related to Midcontinent rift.

---

Corresponding author: Pranshu Ratre, [pranshu.ratre@ou.edu](mailto:pranshu.ratre@ou.edu)

**Abstract**

The southern Granite-Rhyolite province contains a comprehensive record of lithospheric evolution in North America. During the last decade, increased seismicity along with improved seismic monitoring installations in Oklahoma provided a rich catalog of local earthquakes. The source-receiver geometry of this dataset is well posed to illuminate the middle and lower crust through long offset recordings of the Pg phase. We present a 3-D P-wave velocity model for central and north Oklahoma developed through a non-standard processing scheme applied to local earthquake waveforms recorded from 2010-2017, focusing on the deeper crust. We employed common-mid-point sorting, stacking, and inversion of Pg-phases which resulted in a set of localized velocity-depth functions up to depths of 40 km. Using this methodology, we significantly increased the S/N ratio for far offset (~250 km) local earthquake waveforms which led to the increase in depth of investigation for our final 3-D velocity model. We find high velocity (> 7 km/s) lower crust throughout the investigated area which suggests a mafic lower crust. The high velocities support previously established models which state that the lower crust of the Granite-Rhyolite province was derived from melting of older crust. We further relate shallow and middle crustal velocity anomalies to other data sets such as gravimetric and magnetic anomalies, and the spatial distribution of earthquakes. We interpret the Nemaha Fault system as a deep-rooted discontinuity which separates two crustal domains. On the contrary, we do not find clear evidence for the existence of the Midcontinent rift (MCR) in northern Oklahoma.

**Plain Language Summary**

To understand how the crust in Oklahoma was created we require information from the deepest, oldest part of the crust. Waves generated by the earthquakes can be used to image the Earth's crust. The farther these waves travel, more noise is added to the data. Our technique minimizes the noise and enhances the signal observed even at stations greater than 200 km away from the earthquake source. This helps in deriving rock properties for the deepest part of the Earth's crust. Oklahoma has recently seen an exponential increase in the number of earthquakes due to oil and gas production activities. Spatially, they cover a large area in central Oklahoma, thus providing dense subsurface information in this region. We use these earthquakes and apply our technique to derive velocities of the Primary waves (P-waves) in the rocks. We observe velocity variations that indicate in-

43 trusive structures in the upper crust. We also observe high P-wave velocities for the lower  
44 crust which indicates that the crust is composed of high-density material. Our 3-D P-wave  
45 velocity model provides insights into the nature of the crust and also gives a deeper and  
46 more detailed picture of the regional crustal structures in Oklahoma.

## 47 **1 Introduction**

48 The study of Precambrian rocks in the midcontinent region (Figure 1) of North  
49 America is crucial in understanding the Proterozoic evolution of the North American con-  
50 tinental lithosphere. Due to the limited exposures of the Precambrian crystalline rocks in  
51 the midcontinent region, most studies have used cores and drill cuttings to study the Pre-  
52 cambrian geology in this region. In Oklahoma, the Precambrian basement is covered by  
53 Phanerozoic sediments except for a small area in the northeast and in the eastern Arbuckle  
54 mountains in the southeast.

55 Some of the early petrological and geochronological studies of the Precambrian  
56 basement rocks laid the groundwork for addressing the continental evolution in the mid-  
57 continent region (Bickford & Lewis, 1979; Bickford et al., 1981, 1986; Denison et al.,  
58 1984; Lidiak, 1996; Muehlberger et al., 1966, 1967; Nelson & DePaolo, 1985). U-Pb  
59 zircon geochronological studies from outcrop and drill cuttings established the age of  
60 these rocks to be about 1.4-1.34 Ga in the southern midcontinent (Bickford et al., 1981;  
61 Muehlberger et al., 1967). Nelson and DePaolo (1985) differentiated the rocks in the Granite-  
62 Rhyolite provinces based on Sm-Nd isotopic studies. Their “Nd-line” defines an isotopic  
63 boundary that divides the granite-rhyolite provinces based on the model ages, where rocks  
64 in the northwestern part are derived from older cratonic rocks (1.8-1.6 Ga) while rocks  
65 in the southeast of the Nd-line, from juvenile rocks (1.5-1.3 Ga) (Figure 1). Denison et  
66 al. (1984) used petrographic analysis to further divide the Precambrian basement rocks  
67 in northeastern Oklahoma. These early studies were instrumental in establishing the ages  
68 and extent of the Granite-Rhyolite province in the midcontinent but are based on outcrop  
69 and drill cuttings, and they are unable to describe the nature of the lower crustal rocks.  
70 Lack of coeval xenoliths in the midcontinent region has further contributed to our lack of  
71 knowledge of deeper crust in this region. Figure 1 shows the major tectonic provinces and  
72 crustal features in the midcontinent region.

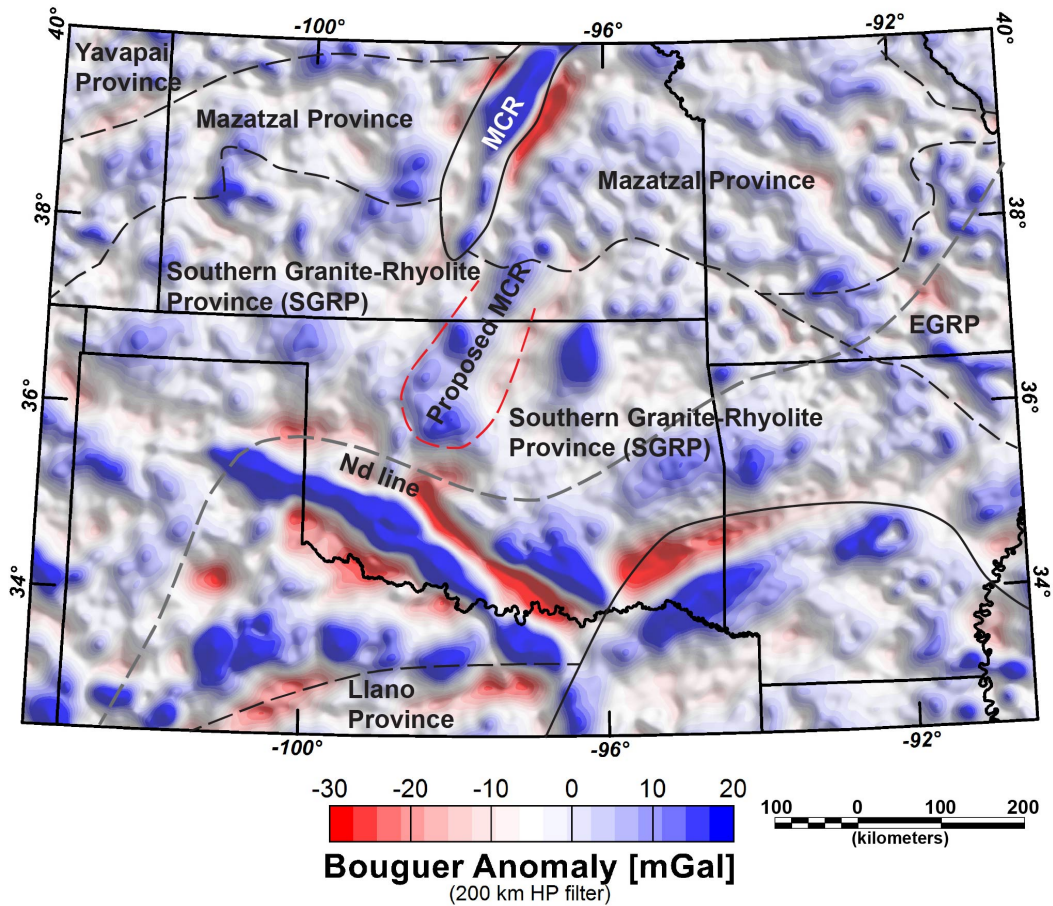


**Figure 1.** Tectonic provinces in the central part of the midcontinent (Modified from Bickford et al. (2015)). Bouguer gravity anomalies (based on Decade of North American Geology (DNAG) data) are shown after applying a 200 km high-pass wavelength filter to suppress upper mantle features. A possible continuation of the Midcontinent rift (MCR) in Oklahoma is shown as proposed by previous studies (see text for details). [EGRP: Eastern granite-rhyolite province].

73 While the earlier workers were able to establish the vast extent of this volcanic province,  
 74 its origin has been debated for decades. Presence of A-type plutons further adds to the  
 75 enigma of its origin (Anderson & Bender, 1989; Bickford et al., 2015; Denison et al.,  
 76 1984). Based on the studies of these plutons and rocks from the granite-rhyolite provinces,  
 77 several theories including extensional anorogenic settings, back-arc magmatism related  
 78 to early Grenville orogeny, and back-arc and intracontinental magmatism related to ac-  
 79 cretionary tectonism in Laurentia of 1.6-1.3 Ga, have been considered (Amato et al.,  
 80 2011; Anderson & Bender, 1989; Whitmeyer & Karlstrom, 2007). Recent Lu-Hf studies  
 81 by Bickford et al. (2015), provide a new model for the formation of the granite-rhyolite

82 province of the midcontinent. Their isotope data corroborates the presence of Nd-line as  
83 given by Nelson and DePaolo (1985). They suggest basaltic underplating as part of the  
84 mechanism that led to the melting of lower crustal rocks that intruded to form the granite-  
85 rhyolite provinces. Evidence for basaltic underplating can be interpreted as high velocity  
86 (P-wave velocity 6.9-7.5 km/s) lower crustal layer, as observed for e.g. by Karlstrom et al.  
87 (2005) and Thybo and Artemieva (2013) through deep crustal seismic velocity models in  
88 other parts of the world. However, such deep crustal seismic studies with sufficient verti-  
89 cal and horizontal resolution are scarce for the Granite-Rhyolite province.

90 Another intriguing feature in the midcontinent is the ~3000 km long Midconti-  
91 nent rift (MCR), a failed rift that formed ca. 1.1 Ga within Laurentia (Hinze et al., 1997;  
92 Van Schmus & Hinze, 1985). During the 20-40 Myr rifting event, vast amounts of ig-  
93 neous rocks followed by sedimentary rocks were deposited within the rift. The signatures  
94 of Midcontinent rift are observed as high gravity anomalies stretching from the Great  
95 Lakes to central Kansas (Hinze et al., 1997; Sims et al., 2005; Van Schmus & Hinze,  
96 1985). Several authors extend the MCR into north central Oklahoma based on relatively  
97 high gravity anomalies that appear to continue from the gravity anomalies observed in the  
98 north (Kolawole et al., 2020; C. A. Stein et al., 2014, 2015) (Figure 1). Unlike modern  
99 rifts where decreased crustal thickness due to extension is observed (Thybo & Artemieva,  
100 2013), crustal thickening is observed for the northern part of the MCR (Chichester et  
101 al., 2018; Hinze et al., 1997; Shen et al., 2013; Zhang et al., 2016). Increased crustal  
102 thickness is attributed to a compressive event that inverted the rift, after it had already  
103 failed (C. A. Stein et al., 2015, 2018). Studies by Chichester et al. (2018) and Zhang et  
104 al. (2016) were conducted in the northern, more prominent part of the MCR. There is evi-  
105 dence for underplating beneath the MCR in certain regions (Chichester et al., 2018; Woelk  
106 & Hinze, 1991; Zhang et al., 2016). Surface evidence for the rift is not observed in Ok-  
107 lahoma, and so deep crustal studies that reveal the seismic structure can inform about the  
108 presence or absence of the rift feature in Oklahoma.

109 Despite emphasis on seismic studies for hydrocarbon exploration in its sedimentary  
110 basins, Oklahoma is significantly under-explored by means of deep crustal-scale seismic  
111 imaging campaigns. Consequently, knowledge of the deep crustal structure is limited and  
112 constrained to a few locations only. The recent increase in induced seismicity due to oil  
113 and gas production (Ellsworth, 2013; Keranen et al., 2014) and the subsequent efforts  
114 in instrumentation to monitor this activity, which also coincided with the ongoing de-

115 ployment of US transportable array across United States, resulted in a large-scale passive  
116 seismic experiment, albeit unintentional. We make use of local earthquake data recorded  
117 across 10 networks between 2010-2017 to develop a 3-D P-wave velocity model of the  
118 crust for central Oklahoma, a core part of the Precambrian midcontinent crust. As the sta-  
119 tion coverage and earthquake distribution resembles an irregular 3-D active seismic exper-  
120 iment, we employ active seismic processing techniques of common mid-point sorting and  
121 stacking to the local earthquake waveforms. This improves the signal-to-noise ratio and  
122 simplifies the wavefields of the recorded data, allowing for imaging of deeper structures  
123 and large areas. Our study aims to contribute to understanding the evolution of this under-  
124 studied part of the midcontinent crust. Furthermore, we suggest a workflow for processing  
125 local earthquake data which is potentially applicable to other areas as well. In this paper  
126 we present and discuss our methodology and geologic and tectonic implications from our  
127 derived 3-D seismic model.

## 128 **2 Regional Geology and Previous Geophysical Studies**

### 129 **2.1 Geology**

130 The evolution of Laurentia through a periodic and continued accretion of igneous  
131 material via volcanic and island arcs over the Archean cratons is the most widely accepted  
132 model of the formation of lithosphere in the continental United States (Whitmeyer & Karl-  
133 strom, 2007). The Mazatzal Orogeny ca. 1.65-1.6 Ga resulted in the accretion of juve-  
134 nile volcanic arcs forming the older crustal rocks in Oklahoma (Whitmeyer & Karlstrom,  
135 2007). Although the southern extent of the Mazatzal province has not been mapped, iso-  
136 topic evidence by Nelson and DePaolo (1985) and core and outcrop evidence from sur-  
137 rounding states of New Mexico and Kansas suggest an extension of this province beneath  
138 the Granite-Rhyolite province of Oklahoma (Anderson & Bender, 1989; Whitmeyer &  
139 Karlstrom, 2007).

140 The Mazatzal orogeny was followed by the accretion of the Southern Granite-Rhyolite  
141 province (SGRP) ca. 1.5-1.35 Ga. The Sm-Nd isotopic study by Nelson and DePaolo  
142 (1985) provided a major breakthrough in understanding the origins of SGRP. Their stud-  
143 ies lead to the conclusion that these rocks were derived from older crustal rocks. This  
144 study was further supported by Van Schmus et al. (1996) who calculated Sm-Nd model  
145 ages showing the Mesoproterozoic rocks of SGRP with a consistent increase in age mov-

146 ing from southeast to northwest. The tectonic setting of the SGRP and the coeval A-  
147 type plutons have been studied and evaluated by various workers. Whitmeyer and Karl-  
148 strom (2007) suggest a convergent and transpressional setting wherein the emplacement  
149 of Granite-Rhyolite province was caused by a tectonic episode away from the plate mar-  
150 gins. Amato et al. (2011) suggest an extensional or transpressive setting for the Granite-  
151 Rhyolite terrain based on their studies of granitic plutons in Burro Mountain, New Mex-  
152 ico, which are coeval with the basement rocks of Oklahoma. Studies based on A-type  
153 plutons indicate an anorogenic origin, suggesting the source of these plutons as partial  
154 melting of juvenile crust (Anderson & Bender, 1989). A recent study by Bickford et al.  
155 (2015), presents new geochronological and isotopic data for samples across the mid-continent  
156 region of United States. Their zircon age studies revealed that the continental scale mag-  
157 matism was long lived (150-200 Ma) and locally episodic as given by the bimodal zircon  
158 age distribution in the midcontinent (Bickford et al., 2015). Lack of zircon in many sam-  
159 ples analyzed by Bickford et al. (2015), along with magma temperatures derived from the  
160 existing zircon samples suggest temperatures above 850 °C. Their conclusions are sim-  
161 ilar to study by Goodge and Vervoort (2006), who analyzed Hf isotope compositions in  
162 the zircons in samples from Penokean (1.9-1.8 Ga), Mojave (1.8-1.7 Ga), Yavapai (1.8-  
163 1.7 Ga), and Granite-Rhyolite (1.5-1.3 Ga) provinces. Studies of A-type plutons also sug-  
164 gest their formation from partial melting of tholeiitic magma (Frost & Frost, 2011, 2013;  
165 Shaw et al., 2005). Bickford et al. (2015) suggest a convergent plate boundary model at  
166 the northeastern margins of Laurentia that led to creation of back arcs in the continen-  
167 tal interior. They argue that the convergent active margin can lead to destabilization of  
168 the back arcs. This can cause delamination of the lithosphere, consequently leading to a  
169 shallower lithosphere-asthenosphere boundary and higher temperatures at shallower depths  
170 which may induce crustal melting. This model seems to agree with the models suggested  
171 by Karlstrom et al. (2001), Slagstad et al. (2009), and Whitmeyer and Karlstrom (2007).

172 The Precambrian accretion of the crust was followed by opening of the Iapetus Ocean  
173 in late-Neoproterozoic - early-Cambrian and the formation of the Southern Oklahoma  
174 Aulacogen (SOA) (Gilbert et al., 1993; Buckley, 2012; Thomas, 1991; Whitmeyer & Karl-  
175 strom, 2007). SOA comprises of the Wichita uplift, the Arbuckle uplift and the Anadarko  
176 basin. The evolution of these structures continued through the Cambrian through, contin-  
177 ued subsidence, deposition, erosion, and intrusion of igneous rocks (Keller et al., 1983).  
178 Finally, intense deformation and erosion during the Pennsylvanian associated with the An-

179 central Rockies orogeny led to the present-day configuration of the tectonic features, in-  
 180 cluding the Nemaha Uplift, we observe today in Oklahoma (Figure 2) (Garner & Turcotte,  
 181 1984; Gilbert et al., 1993; Johnson, 2008).

182 Gravity and magnetic data can provide some information on the crust (Bickford et  
 183 al., 1986; Van Schmus et al., 1996; Sims et al., 2005), but non-uniqueness of these meth-  
 184 ods require constraints such as seismic data to infer robust interpretations. The lack of  
 185 rock samples from deeper crust in Oklahoma further limits our understanding of this part  
 186 of the crust.

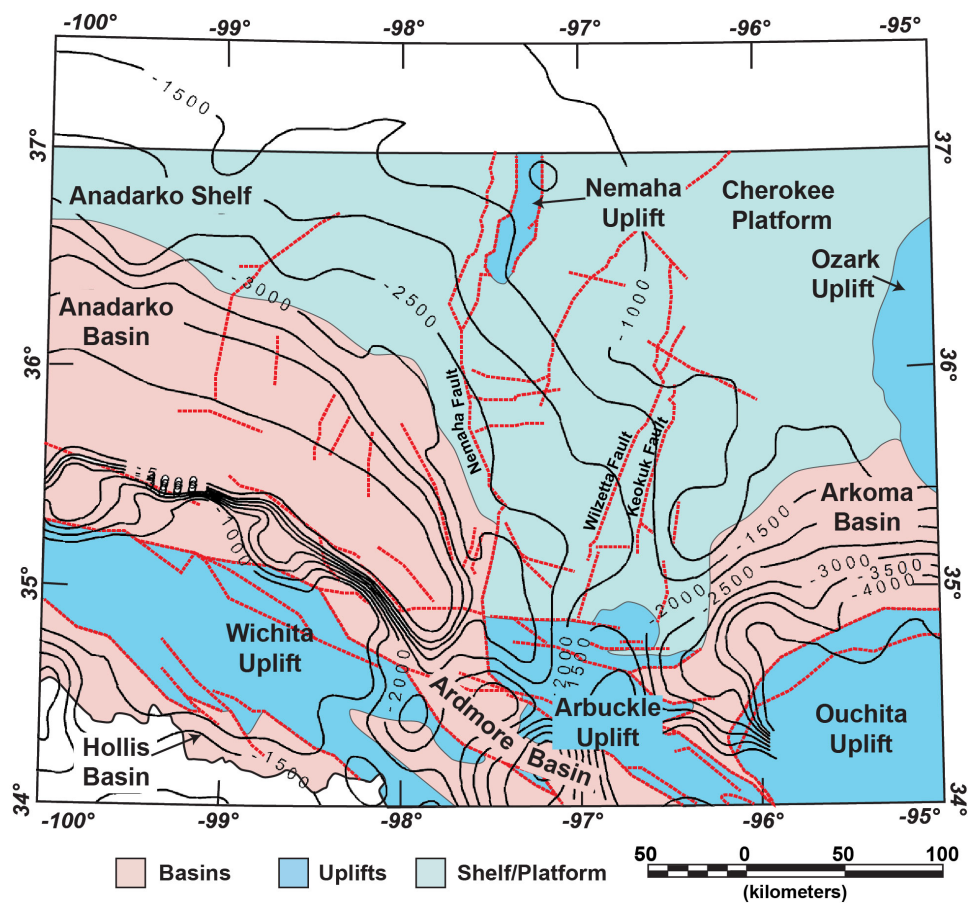


**Figure 2.** Major tectonic features in Oklahoma (adapted from Northcutt and Campbell (1996)). Red dashed lines: major fault systems. Black solid lines: depth-to-basement contours (meters) computed from basement well information as given by (Campbell & Weber, 2006).

## 2.2 Previous Seismic Studies

Tryggvason and Qualls (1967) derived a simple layered model for Oklahoma's crust through a 2-D active seismic refraction study. The ~450 km profile runs northeast-southwest across Oklahoma, cutting through different tectonic units (Figure 3). Based on recordings of multiple shots at 2 shot points in Chelsea, NE Oklahoma, and Manitou, SW Oklahoma, at 26 seismometers between the shot points, they interpreted a homogeneous three-layer earth model and provided the first look at the depth of Moho and crustal velocity variations in Oklahoma. The same 2D line was re-processed and integrated with other datasets by Mitchell and Landisman (1970) who derived a more detailed crustal model. They used seismic refraction and reflections observed from the Tryggvason and Qualls (1967) - 2D profile, gravity anomaly data, basement depth data, and well-log data. Their final velocity model showed homogeneous crustal layers below the upper crust (up to 18 km). They modelled the shallow upper crust in much greater detail as compared to the earlier model and observed discontinuities due to the presence of fault zones cutting through the profile. They interpret the crustal thickness to be between 46 - 46.5 km with P- wave velocities up to 7.39 km/s for the lower crust.

In the late 1970s, deep seismic reflection profiles were shot by Consortium for Continental Reflection Profiling (COCORP) and a 2-D wide angle reflection/refraction survey by University of Texas at El-Paso (UTEP) and University of Texas at Dallas (UTD) in 1985. Both of these surveys aimed to understand the deeper structure of Wichita Uplift and characterize structural features at the boundary of Southern Oklahoma Aulacogen and the Anadarko Basin. Several authors worked on developing a 2D velocity structure across Wichita uplift and Anadarko basin using this data (e.g. Agena et al., 1989; Brewer et al., 1983, 1984; Brewer & Oliver, 1980; Phinney & Jurdy, 1979; Zhu & McMechan, 1989, and others.). These investigations revealed a layered basement about 12 km thick and a thick crust with depth to Moho varying from 40-45 km (Lynn et al., 1981; Pratt et al., 1992). The UTEP-UTD seismic survey was reanalyzed by Buckey (2012), who was able to identify more reflections. The author further used gravity data to obtain a detailed velocity and geologic model for the upper – mid crust up to 20 km depth. They report a deeper Precambrian basement as compared to Pratt et al. (1992), overlain by metasediments, rift fill and Proterozoic basin fill. Figure 3 shows locations of the various active seismic surveys conducted in Oklahoma.

219 There have been a few passive seismic studies targeting large scale crustal structure  
220 in Oklahoma. Local earthquake tomography by Chen (2016) and Toth (2014) obtained up-  
221 per crustal (up to 15-20 km) seismic velocity. Velocity anomalies observed in these mod-  
222 els show close correlation to the major tectonic features like the Nemaha Fault Zone and  
223 the Wilzetta Fault Zone in Oklahoma. A high resolution but shallow anisotropic Pg ve-  
224 locity was developed for central Oklahoma by Pei et al. (2018). It shows lateral velocity  
225 variations in the uppermost crust (5-10 km). Receiver function analysis and Pn tomogra-  
226 phy by Tave (2013) using the data from US transportable array network revealed deeper  
227 discontinuities like Moho and Hales discontinuity. The author presents depths to the Moho  
228 between 36 km and 42 km throughout the state. McGlannan and Gilbert (2016) reported  
229 a crustal depth variation from 30-55 km across the state of Oklahoma, which they calcu-  
230 lated from the Earthscope Automated Receiver Survey using the US transportable array.  
231 In general, the passive seismic studies conducted in Oklahoma so far either do not have  
232 the necessary depth of investigation to image the deeper crustal structures (Chen, 2016;  
233 Toth, 2014), or lack the resolution required to be able to comment on the regional crustal  
234 structure (Evanzia et al., 2014; McGlannan & Gilbert, 2016). Our methodology aims to  
235 address these problems and obtain a deeper seismic model that can highlight the regional  
236 crustal features in Oklahoma.

### 237 **3 Data and Methodology**

238 Local earthquakes are commonly used for imaging in seismically active regions.  
239 Local earthquake tomography (LET) uses travel times of earthquake phases to invert for  
240 the velocity structure, while often simultaneously (re-)locating the earthquake source (e.g.  
241 Kissling et al., 1994; Rawlinson & Sambridge, 2003). The term ‘local’ refers to a spatial  
242 overlap between sources and receivers, e.g. the receiver array should enable the recording  
243 of crossing rays at all incidence angles, and therefore allow for a tomographic inversion  
244 for both velocity structure and hypocenters.

245 Earthquake depths play a crucial role for the depth of investigation in LET. For a  
246 given velocity gradient, waves from shallow earthquakes recorded at large offsets reveal  
247 information from the deeper crust, while deep earthquakes record deep crustal information  
248 at short offsets due to their sub-vertical ray paths (Braeuer et al., 2012; Tong et al., 2017).  
249 The signal-to-noise (S/N) ratio also decreases with offset (source-receiver-distance) for  
250 both shallow and deep local earthquakes, which ultimately leads to a lower depth of in-

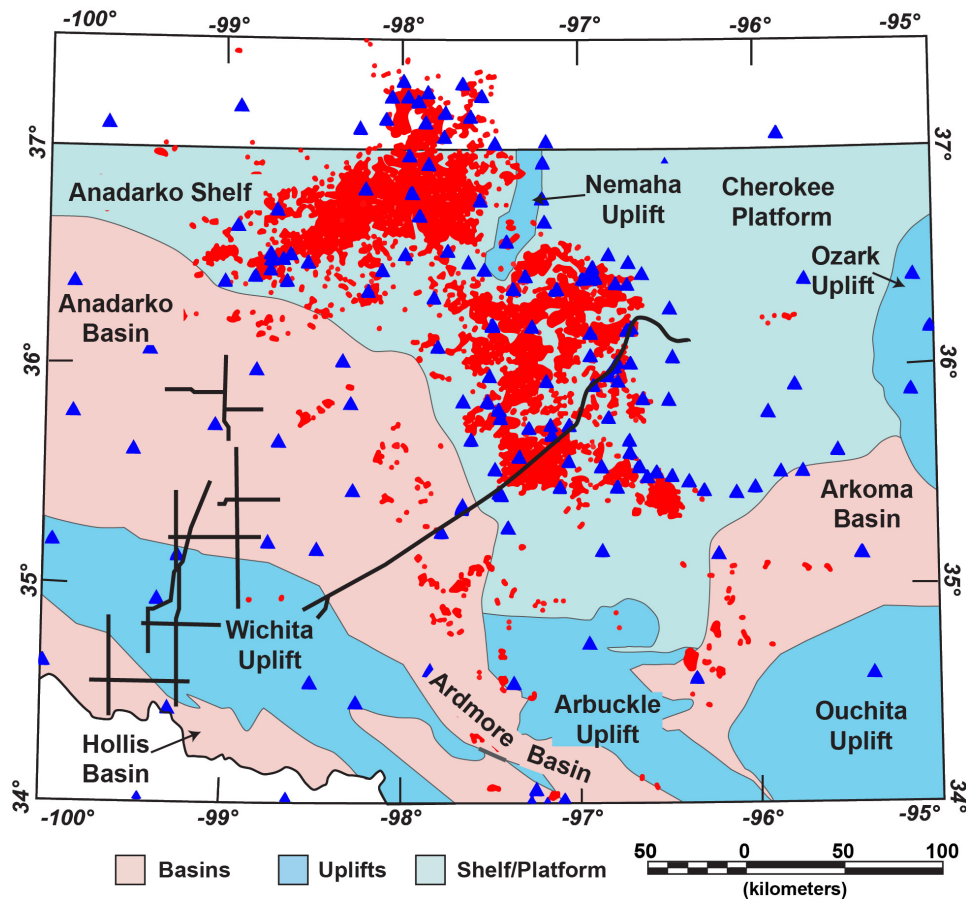


**Figure 3.** Black thick lines: previous active seismic studies conducted in Oklahoma for crustal investigations. Red dots: location of earthquakes used in this study. Blue triangles: stations used in this study.

251 vestigation when using shallow earthquakes only. The traditional LET approach involves  
 252 identifying and picking seismic phases across different stations. Sparse distribution of  
 253 recording stations is common in passive seismic network geometries and makes correct  
 254 phase correlation and identification difficult. Estimating robust travel times at large off-  
 255 sets is challenging, in particular for small magnitude events. Consequently, traditional LET  
 256 methods in Oklahoma where the earthquake depths are shallow ( $\sim 2\text{-}7$  km depth) (Figure  
 257 S1) can only represent velocity variations in the upper crust (Chen, 2016; Toth, 2014).  
 258 Interpretation of individual travel times requires data of high quality, and in the case of  
 259 many observations, (semi-)automated phase correlation and picking routines (Chen, 2016;  
 260 Thybo et al., 2006).

261 To overcome the issues of low S/N ratio and ambiguous phase correlations, we pro-  
 262 pose to stack waveforms and apply specifically designed processing and inversion rou-

263 tines. This approach has been successfully applied to active source 3-D wide-angle refrac-  
264 tion/reflection (WAR/R) data as well as earthquake sources to both P- and S-wavefields  
265 (Behm, 2009; Behm et al., 2007; Buehler & Shearer, 2013; Loidl et al., 2014). We use  
266 existing localizations of the events (Schoenball & Ellsworth, 2017) and consider the data  
267 set as an active 3-D acquisition with irregular geometry. Using the principle of reciprocity,  
268 the small number of recording stations is compensated by a large number of events. We  
269 aim for stacking and inversion of Pg (refractions from the crust) phases to derive a 3-D P-  
270 wave velocity model of the crust. Stacking is preceded by sorting to common-mid-point  
271 (CMP) gathers, as wide-angle refractions best approximate the seismic structure at the  
272 common-midpoint location where the ray travels horizontal. Pre-stack processing aim at  
273 enhancing and simplifying the wavelets such that the under-sampled wavefields can stack  
274 constructively. Stacking has a tendency to favor robust models, that is relative insensitiv-  
275 ity to randomly distributed data outliers (Behm et al., 2007). CMP regionalization leads  
276 to a set of local 1-D travel time curves approximating the crustal structure at the CMP lo-  
277 cation. Those travel time curves are picked and inverted, and the derived set of local 1-D  
278 velocity models is eventually combined into a smooth 3-D Pg velocity field.

### 279 **3.1 Data**

280 We use 27,568 local earthquakes recorded at 165 broadband stations belonging to 6  
281 different networks across Oklahoma (Figure 3). The earthquake events were recorded be-  
282 tween the time period January 2010 to September 2017. We use a catalogue which com-  
283 bines relocation from Schoenball and Ellsworth (2017) and HypoDD corrected catalogue.  
284 Hypocenter solutions (including origin time) in those catalogs are associated with uncer-  
285 tainties, which will be addressed in section 3.2.4. Earthquake depths vary from 2-7 km  
286 and we select the maximum epicentral distance for P-wave velocity evaluation to be 250  
287 km. Finally, we have 1,214,112 individual seismic traces that we use for further process-  
288 ing. Station information and earthquake events used are provided in data set S1 and S2.

### 289 **3.2 Pg Processing**

290 The workflow to derive a 3-D crustal P-wave velocity from the Pg phase comprises  
291 six steps:

- 292 1. Geometric and kinematic corrections to account for varying source depths and sedi-  
293 mentary thickness at the receiver locations.
- 294 2. Pre-stack signal processing to increase the S/N ratio and to facilitate constructive  
295 interference.
- 296 3. CMP sorting and stacking in offset bins to derive local 1-D travel time curves.
- 297 4. Manual picking of the 1-D travel time curves.
- 298 5. Inversion of 1-D picked travel time curves for local 1-D velocity-depth functions  
299 representing the CMP location.
- 300 6. Combination of all 1-D velocity models into a 3-D velocity model.

### 301 ***3.2.1 Geometric and Kinematic Corrections (Datuming)***

302 Time and geometric corrections are required to account for the different earthquake  
303 depths and sedimentary thickness at the receiver locations. First, to correct for the eleva-  
304 tion difference between source and receiver of each earthquake-receiver pair, we choose  
305 the corresponding earthquake depth as datum and apply time and offset corrections to  
306 shift the receiver to this datum. Second, stacking of different source-receiver pairs requires  
307 all data to be at the same reference level. We choose a depth of 5 km as our final datum  
308 since most of the earthquakes in Oklahoma are within ~5-7 km depth range (Figure S1).  
309 This introduces further time corrections and offset shifts for both the source and receiver  
310 locations.

311 Datum corrections for wide-angle refractions depend on the earthquake depth, source-  
312 receiver offset, basement structure at source and receiver, and the regional velocity struc-  
313 ture. As opposed to simple static corrections for steep-angle reflections, the combined ef-  
314 fects of velocity structure, basin geometry and velocities, and offset dependency introduce  
315 a high degree of nonlinearity. Calculation of exact time and geometric corrections would  
316 require a 3-D velocity model of the crust, which we do not have at this stage. As an ap-  
317 proximation for the purpose of those corrections, we use a 1-D velocity model for the  
318 crust below basement based on the Christensen and Mooney (1995) model for continental  
319 shields. A 1-D velocity model for the sedimentary cover above basement is taken from the  
320 OGS velocity model for Oklahoma (Darold et al., 2015). An extrapolated basement depth  
321 map calculated from basement penetrating wells and regional gravity data (Campbell,  
322 2007) is used to derive the basement depths at each source and receiver location. We cal-

323 culuate offset-dependent time and offset corrections for a range of earthquake depths and  
324 receiver basement-depths using the raytracing code ANRAY (Gajewski & Pšenčík, 1987;  
325 Gajewski & Pšenčík, 1989). Finally, those corrections are interpolated for the actual earth-  
326 quake and receiver locations for each source-receiver pair. The corrections are largest for  
327 shallow offsets and deep earthquakes (Figure S2).

### 328 **3.2.2 Pre-stack Signal Processing**

329 We apply a minimum phase Ormsby bandpass filter with corner frequencies of 2-4-  
330 6-8 Hz to increase the S/N ratio. To facilitate constructive interference of the Pg phase,  
331 we convert the data to their envelope (modulus of the complex trace). Bandpass filtering  
332 and envelope calculation also lifts the requirement of instrument response removal. This  
333 step is crucial since the receiver spacing is large, and wavelets from different events can-  
334 not be expected to be in phase after CMP sorting. We further increase the visibility of  
335 the Pg phases, in particular at larger offsets, by applying the STA (short-term average) to  
336 LTA (long-term average) ratio signal detection algorithm (Astiz et al., 1996). The averag-  
337 ing windows used for STA and LTA are 0.1 s and 10 s respectively and have been decided  
338 after testing. Figure 4 shows the result of pre-stack signal processing on one event gather.

### 339 **3.2.3 CMP Sorting and Stacking**

340 The signal-processed traces are sorted into common mid-point (CMP)-gathers and  
341 stacked in offset bins. The study area is divided into cells such that the traces whose CMPs  
342 fall into a particular defined cell are sorted into one gather. The offset-sorted Pg phases  
343 in this gather represent travel time curve for the velocity-depth function at the cell loca-  
344 tion (Behm et al., 2007). Rectangular cells are centered on a regular grid with 10 km lat-  
345 eral spacing, and the cell size is automatically varied between 10-70 km throughout the  
346 study area depending on the number of traces which fall into each gather. The variable  
347 cell size accounts for the irregular geometry and is smallest in the central part of the study  
348 area (Figure 5). The final location of the cell is calculated as the average location of all  
349 the trace CMPs in the gather, and the cell size represents the average distance of all trace  
350 CMPs to the final cell location.

351 In each CMP gather, the traces are subjected to a linear move-out (LMO) correction  
352 with a velocity of 6 km/s and finally are stacked in 5 km offset bins. The absolute offset

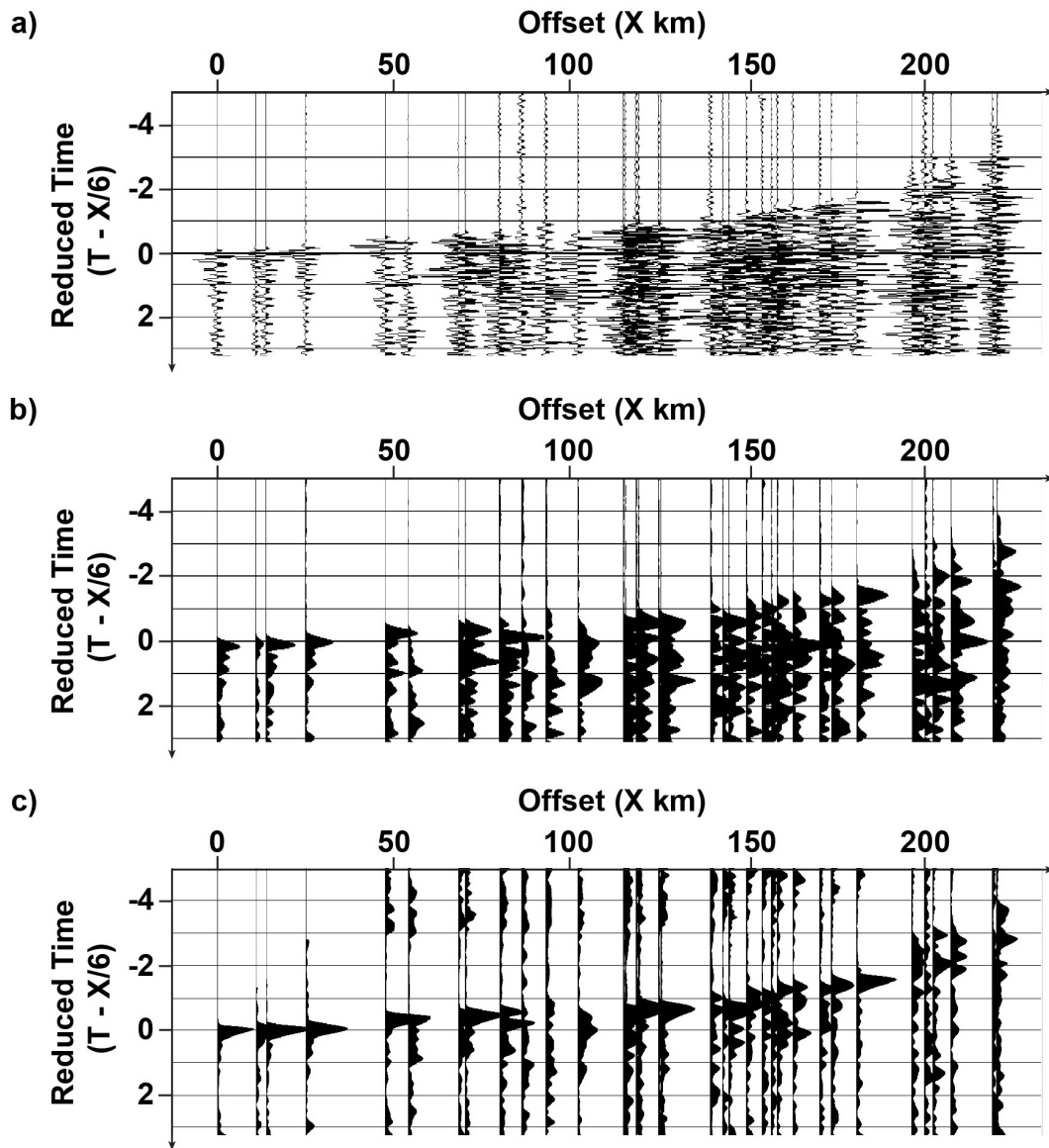


**Figure 4.** Example of preprocessing on one datum-corrected event gather with a linear move-out for a velocity of 6 km/s. a) bandpass filtered (2-4-6-8 Hz), b) signal converted to envelope, c) STA/LTA applied.

353 of each stacked trace is calculated as an average of all traces in the bin. The stacked CMP  
 354 gathers allow for a first qualitative assessment of the influence of the source depths, and  
 355 the errors in event location and origin time as reported in the catalogue. Prior to sorting  
 356 and stacking, we calculate a relative quality value for each event which depends on source  
 357 depth and the hypocenter errors in both depth and lateral position. A large quality value is  
 358 obtained for shallow earthquakes and small errors, and the events are sorted by descending  
 359 quality value. Sorting and stacking are performed on (1) the first 10% of the events (high-

360 quality data only), (2) the first 50% of the events (high to medium quality data), and (3) to  
 361 all events (high to low quality data). Figure 6 shows the trade-off between using a small  
 362 number of high-quality events vs. including a larger number of low-quality events. E.g.  
 363 non-physical humps in the travel time curve and overall low S/N ratio are more effectively  
 364 mitigated in the 50% dataset, which includes earthquakes in the depth range 5 to 7 km.  
 365 Consequently, we chose this data subset for further processing.

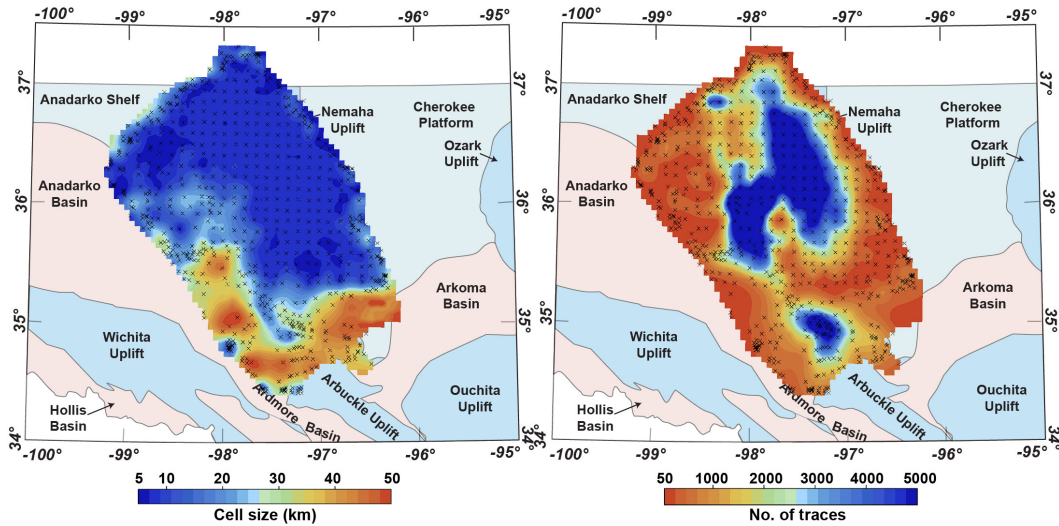


**Figure 5.** (a) size of the CMP bin, (b) number of traces in each CMP bin. CMP bin center locations are shown as “x”.

### 3.2.4 Travel Time Curve Picking

366  
 367 In traditional local earthquake tomography (LET), accurate travel time picks provide  
 368 the arrival times for seismic phases which are then inverted to determine the subsurface  
 369 velocity structure. In contrast, we are picking 1-D travel time curves instead of arrivals  
 370 on individual traces. Before picking is performed all stacked gathers are bandpass filtered  
 371 with a 0.04-0.08-0.5-0.8 Hz Ormsby filter. The stacked gathers have high S/N ratios but  
 372 due to the process of envelope calculation, stacking and low-pass filtering, the phase of  
 373 the waveform is lost. To ensure consistency, we pick smooth arrival time curves along the  
 374 maximum amplitude of the stacked traces. On average, the maximum of the filtered enve-  
 375 lope wavelet corresponds to a theoretical travel-time curve based on a 1-D velocity model  
 376 for continental shields (Christensen & Mooney, 1995). 1-D travel time curves have to rep-  
 377 resent a layer-cake earth model, and as such are more constrained than 3-D travel time

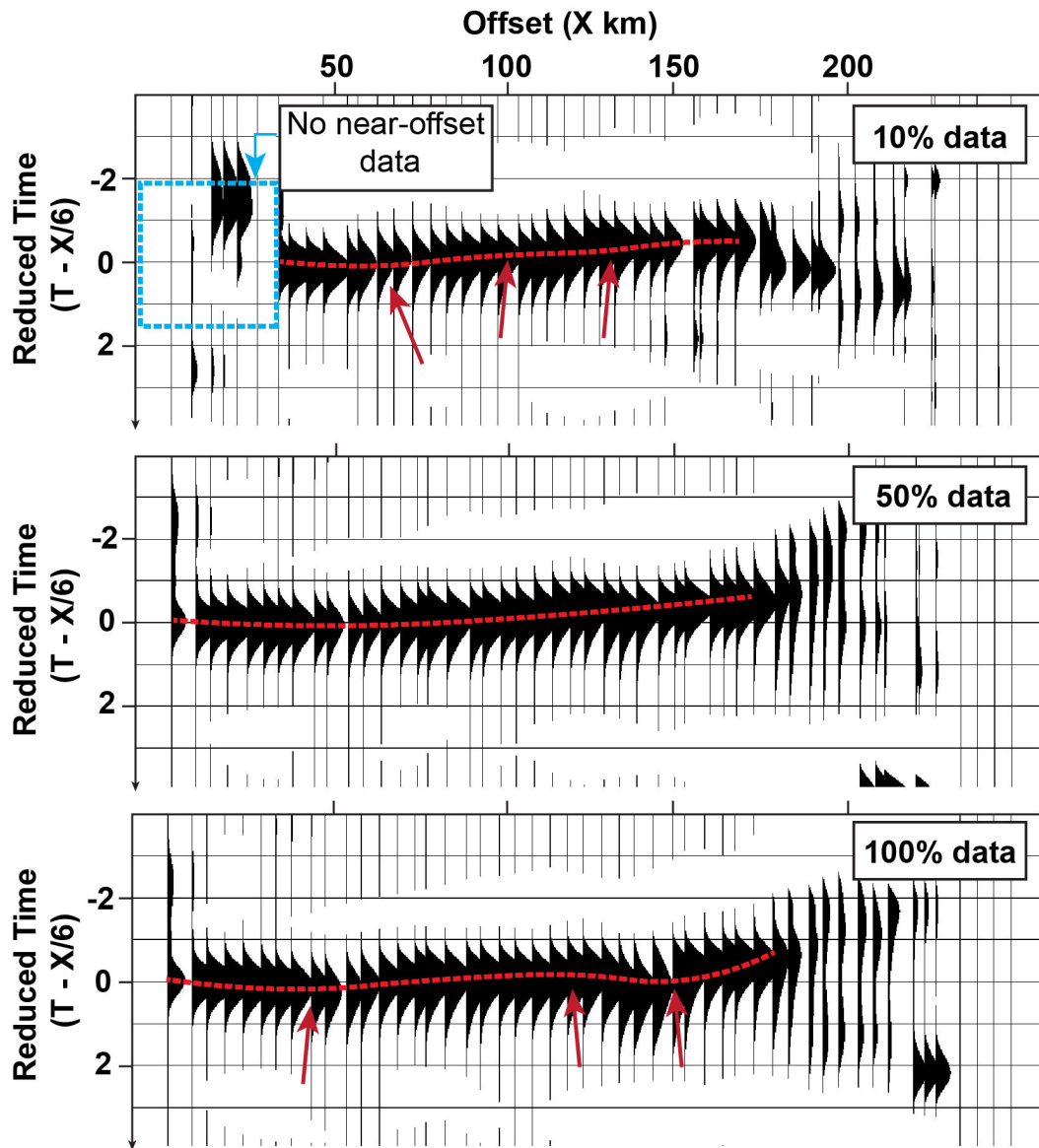


**Figure 6.** Comparing the stacks for 10%, 50%, and 100% data sets (see text for details). Red arrows indicate the unrealistic deviations in the travel time curve for 10% and 100% data sets.

378 curves. This implies that humps or similar (e.g. non-smooth) irregularities in the travel  
 379 time curve should not be picked. Such deviations from a smooth curve may be caused  
 380 by localized gross errors in hypocenter and/or origin time solutions, and we avoid pick-  
 381 ing such arrivals (Figure 7). Continuity and smoothness of the travel-time curve is a re-  
 382 quirement for the assumption of a layer-cake earth model, and introduction of humps in  
 383 the curve will not be representative of geologic structures. A problem resulting from the  
 384 sparse station distribution is a general lack of representative near-offset traces due to the

385 depth of the sources. We only picked smooth travel time curves on stacked gathers where  
 386 enough near-offset traces were available for a stable inversion. Examples for some of the  
 387 stacks and corresponding time-picks are shown in Figure 7. Finally, we manually inspect  
 388 our picks for lateral consistency across the CMP gathers and picks are removed and/or  
 389 corrected if required. We finally obtain 1-D travel time curves representing the velocity-  
 390 depth function at each CMP location.

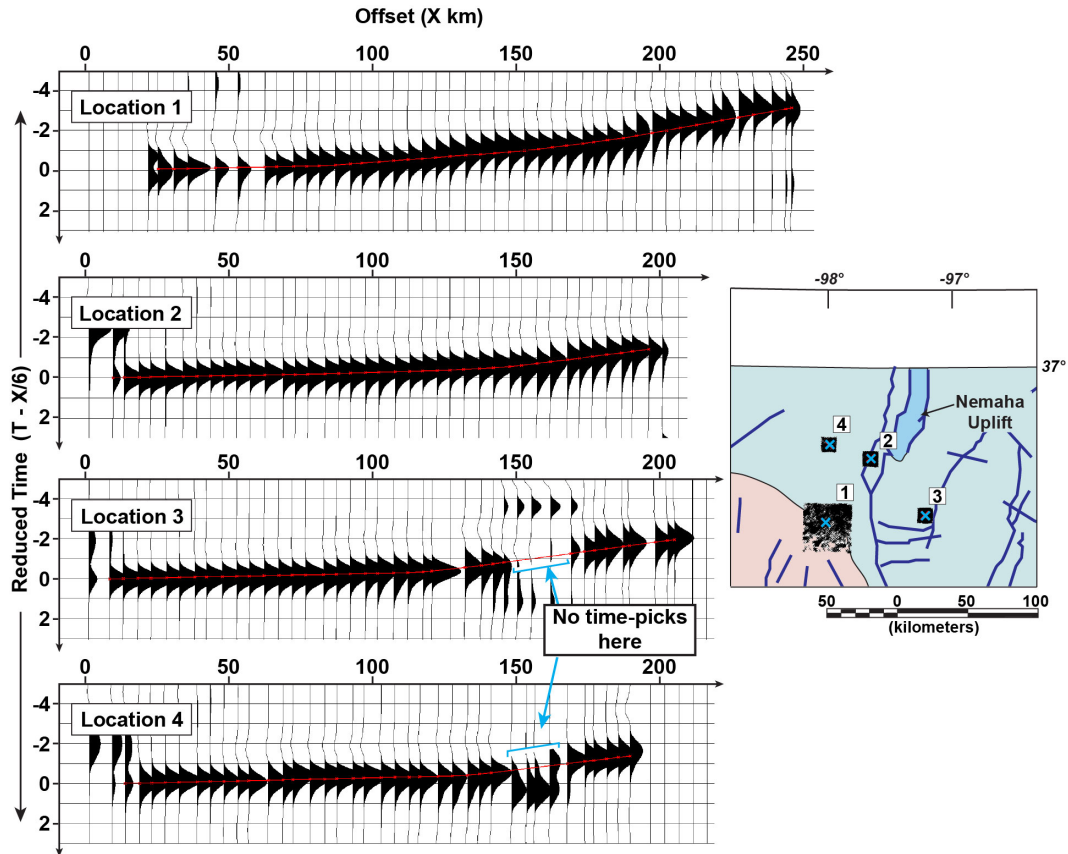


**Figure 7.** Examples of stacks from different locations. The map on the right shows the location and size of CMP bin for each of the stacked gathers. Note the larger CMP bin size for location 1. Small black cross: location of individual CMPs (for each source-receiver pair) within one CMP bin. Blue cross: CMP bin center locations.

391 **3.2.5 1-D Travel Time Inversion and Combination into a 3-D Model**

392 The 1-D travel time curve at each CMP location represents a 1-D velocity-depth  
 393 function at that location. Assuming an initial 1-D velocity model for the crust, the 1-D  
 394 travel time curves are inverted to obtain the velocity information using a ray parameter

395 weighted scheme (Behm et al., 2007). Our initial velocity model is derived from the local  
 396 Oklahoma velocity models for the sedimentary layer (Darold et al., 2015) and the shields  
 397 and platforms velocity model as given by (Christensen & Mooney, 1995) for the basement  
 398 and below. The inversion provides a 1-D velocity-depth function at each location along  
 399 with corresponding resolution elements as the output. The resolution elements define the  
 400 confidence on each of the final computed velocity elements. We also test the robustness of  
 401 our final velocity model based on different initial velocity models (Figure S3). The entire  
 402 workflow (CMP sorting, stacking and travel time picking, inversion) is illustrated in Figure  
 403 8.

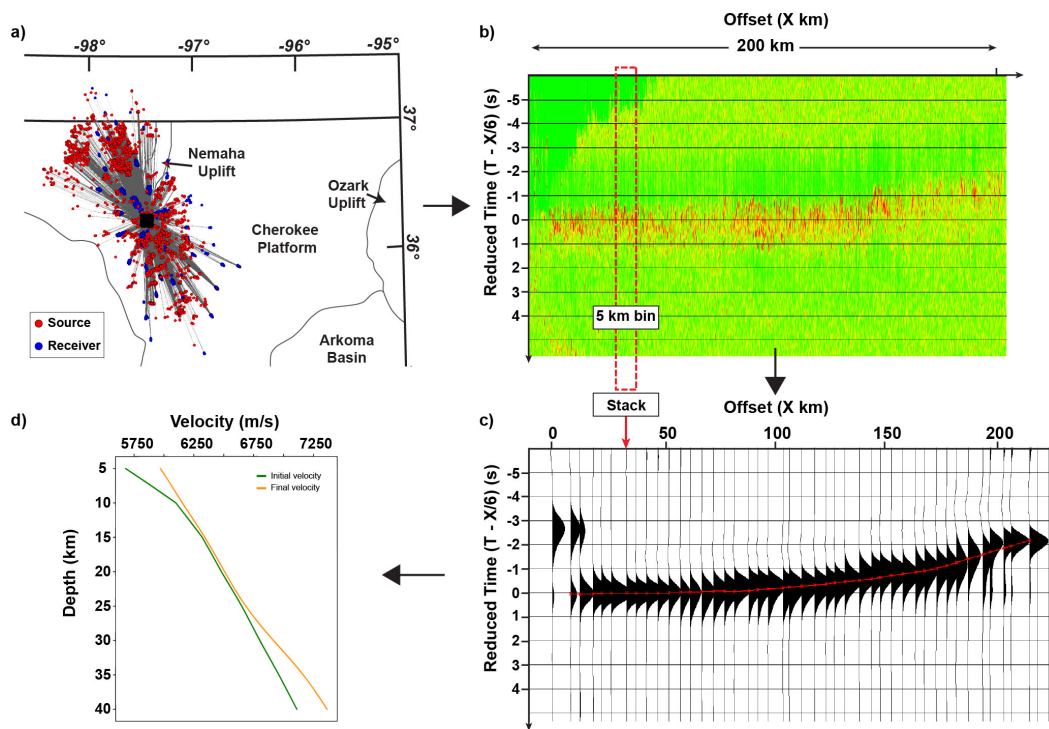


**Figure 8.** Processing steps illustrated for one CMP bin. (a) All source-receiver pairs (grey lines) shown for the CMP bin (black square); (b) Pre-processed earthquake waveforms in this CMP bin arranged according to their offsets with a linear move-out correction of 6 km/s; (c) Stacked gather obtained from 5 km offset-bin stacking of sorted gather in b), red dashed line shows the picked travel time curve; (d) Initial and inverted 1-D velocity model obtained for the CMP bin location.

404 We finally combine the 1-D velocity models derived at each of the CMP locations  
 405 into a 3-D velocity model based on kriging interpolation approach. We present a 3-D ve-  
 406 locity model for Oklahoma that captures regional crustal structures up to depths of ~40

407 km. Average velocities vary from 5.96 km/s at 5 km depth to 7.24 km/s at 40 km with  
408 an overall minimum and maximum of 5.56 km/s and 7.39 km/s respectively. Average ve-  
409 locities for upper-to-middle crust (10-25 km) are very similar to the 1-D global velocity  
410 model as given by Christensen and Mooney (1995) for shields and platform. We observe  
411 higher average velocities for the uppermost crust (5-10 km) and the lower crust (>25 km).  
412 Figure 9 shows combined velocity model as depth slices at 5 km interval starting from 5  
413 km to 40 km. Our velocity model starts at 5 km depth, where we have assumed our pro-  
414 cessing datum. Due to velocity increase with depth, we chose a depth-dependent color  
415 scale in Figure 9 to emphasize lateral variations at each depth. To analyze the velocity  
416 model in more detail we have highlighted regions (Figure 9, Regions A, B, C) which show  
417 velocity anomalies which are discussed in more detail in section 4.

## 418 **4 Discussion**

### 419 **4.1 Comparison with Existing Velocity Models**

420 There have been two major studies that have developed regional velocity models for  
421 the crust in Oklahoma. Chen (2016) developed a 3-D velocity model for the upper crust  
422 (up to ~15 km depth) using traditional travel time tomography applied to local earthquake  
423 waveforms. We are able to co-locate the velocity anomalies mentioned in regions A, B,  
424 and C to the similar velocity anomalies observed in the cross-sections A4 and A5 (Fig-  
425 ure S4) from Chen (2016)'s model. They interpret the high velocity anomalies of region  
426 A as the Midcontinent Rift and regions B and C as intrusions in the crust. The depth of  
427 investigation for their model is limited to about 15 km.

428 The second regional velocity model was developed by Pei et al. (2018) who used a  
429 2-D lateral tomographic technique (Pei et al., 2013) to obtain a high-resolution anisotropic  
430 velocity for the uppermost crust. Their model represents depth-averaged velocities model  
431 for the 5-10 km in the upper crust based on travel times with offsets up to 130 km. We  
432 observe significant differences in some areas when comparing our results to this model.  
433 High velocity anomaly in region A (Figure 9) is not observed in their model, but they  
434 model a very high velocity anomaly just south-east of region A. They also observe less  
435 prominent high velocity anomalies west of region A (Figure 9) high velocity anomaly.  
436 These differences might be related to the different methodologies used in calculating the  
437 velocity models. Pei et al. (2018) chose a data set with epicentral distances varying from

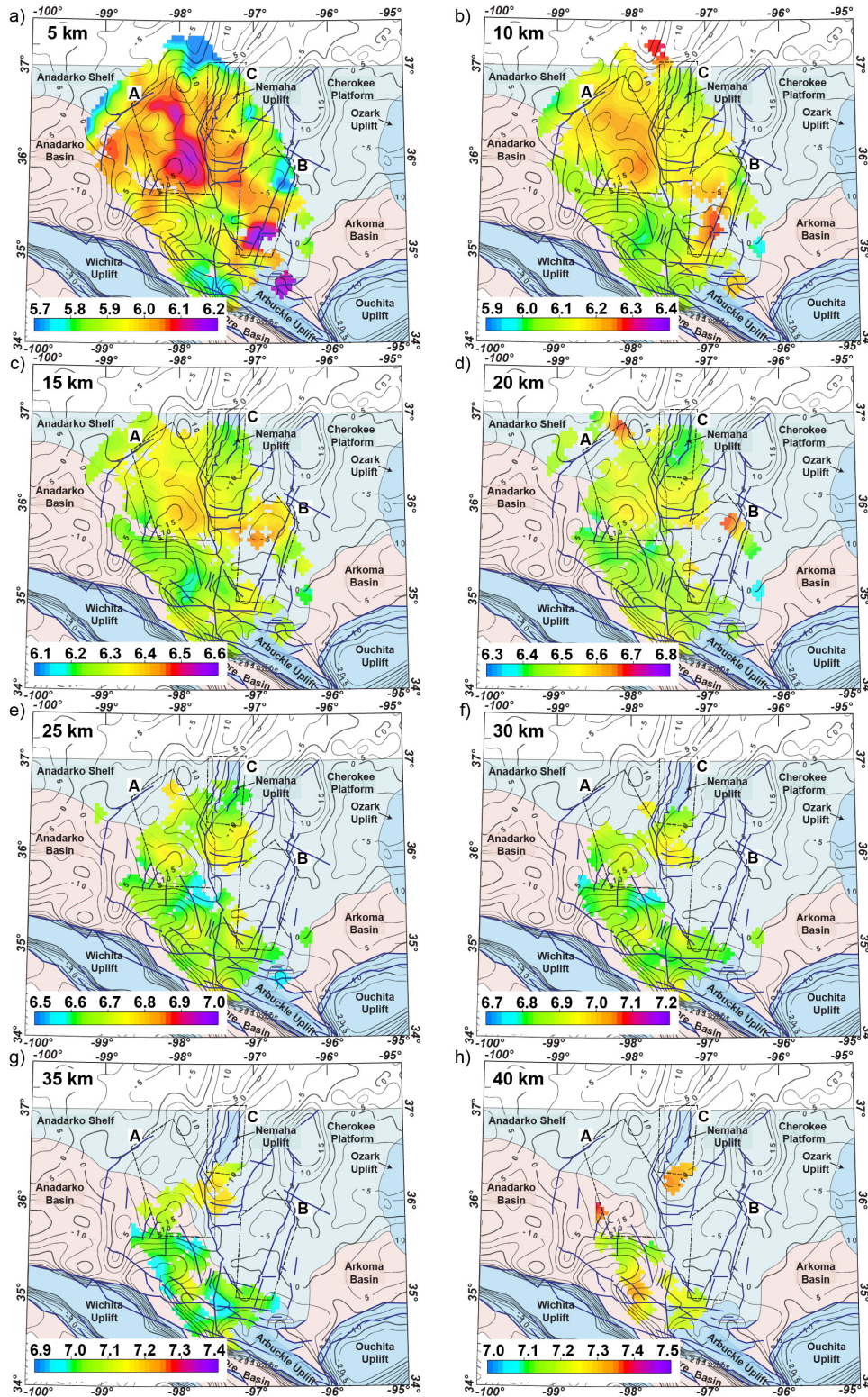


**Figure 9.** Horizontal slices through the 3-D Pg wave velocity model. Note the varying color scale for each depth slice (same range of 500 m/s).

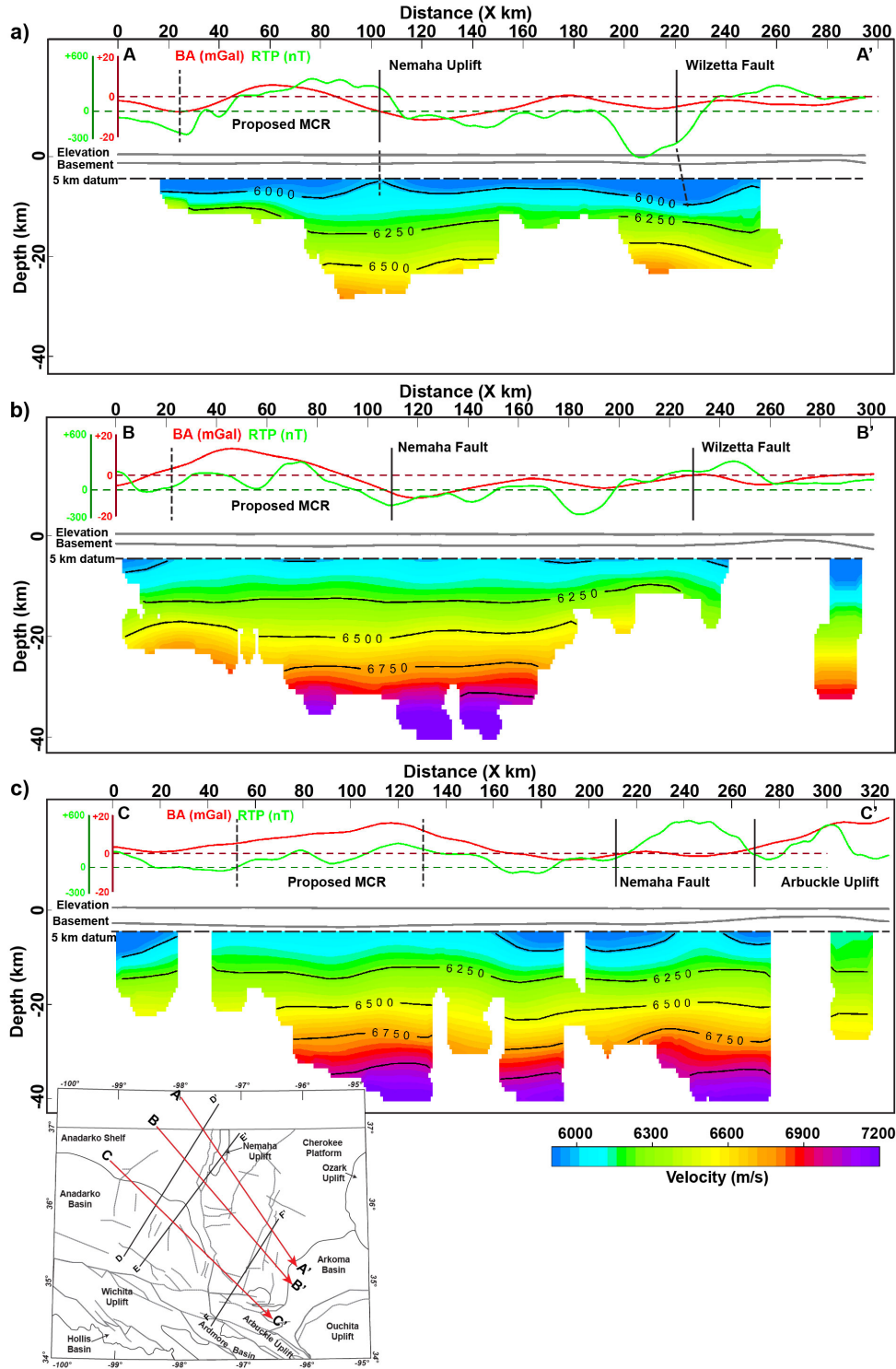
438 ~32 km to ~130 km and assumes a head wave ray path for all the travel times irrespective  
439 of the epicentral distance. As the Pg phase dives down with increasing offset, the head  
440 wave path assumption for offsets as far as 130 km can introduce variations in the final ve-  
441 locity model which may lead to artifacts in velocity imaging. Our calculations show that  
442 the curved ray paths at 120 km offset penetrates down to 15 km depth (Figure S5). As-  
443 suming a head wave geometry, the velocities in the mid-crustal depth range between the  
444 hypocenters and 15 km will be projected to the shallow part of the basement. Another  
445 point of difference is the model assumption of isotropic crust in our model whereas Pei et  
446 al. (2018) considers anisotropy.

## 447 **4.2 Crustal Structures**

448 The upper crust in Oklahoma shows significant lateral velocity variations imply-  
449 ing that the crustal structure in the upper crust is more complex than an overall granitic  
450 basement may suggest. We observe a high velocity anomalies at 5 km depth (Figure 9a;  
451 regions A and B) in roughly NW-SE direction. This prominent high velocity region ex-  
452 tends down to depths of ~15 km (Figure 9b, c; Region A) but decreases in intensity and  
453 lateral extent as the depth increases. Region A appears to be bounded at its eastern side  
454 by the Nemaha fault system. Cross-sections CC', DD' and EE' (Figure 10 c, d, e) show  
455 these high velocity anomalies in the upper crust as well. These high velocity anomalies  
456 correlate with the gravity anomalies. Chen (2016) interpreted this anomaly as an evi-  
457 dence for the extension of the Midcontinent Rift into northern Oklahoma. Our model ex-  
458 tends deeper in this region and we observe that the velocity anomaly is only present in  
459 the upper-middle crust extending down to about 20 km in depth (Figure 9, Figure 10c).  
460 We correlate this high velocity anomaly with the occurrence of intra-basement reflectors  
461 in this region. Several authors (Chopra et al., 2018; Kolawole et al., 2020) have mapped  
462 these reflectors in 3-D (industry) active seismic data in depths between 8 to 10 km and  
463 have interpreted them as mafic sill intrusions (Kolawole et al., 2020). The mafic nature  
464 of these intra-basement reflectors may explain the anomalously high velocity observed in  
465 our model and would suggest mafic layering over a significant larger depth range, as the  
466 industry-scale active source are restricted in their depth extent.

467 We observe another high velocity anomaly in south-central Oklahoma (Figure 9 a,  
468 b, c, d; Region B) which appears more complex. We observe a decreasing intensity in the  
469 southern part with depth while the anomaly in the northern seems to be stronger in the

470 middle crust. The southern anomaly corresponds to a magnetic high (Figure 10f) while  
 471 the northern anomaly corresponds to a magnetic low. The different magnetic signatures of  
 472 the two anomalies indicate differences in lithological composition of the shallow to mid



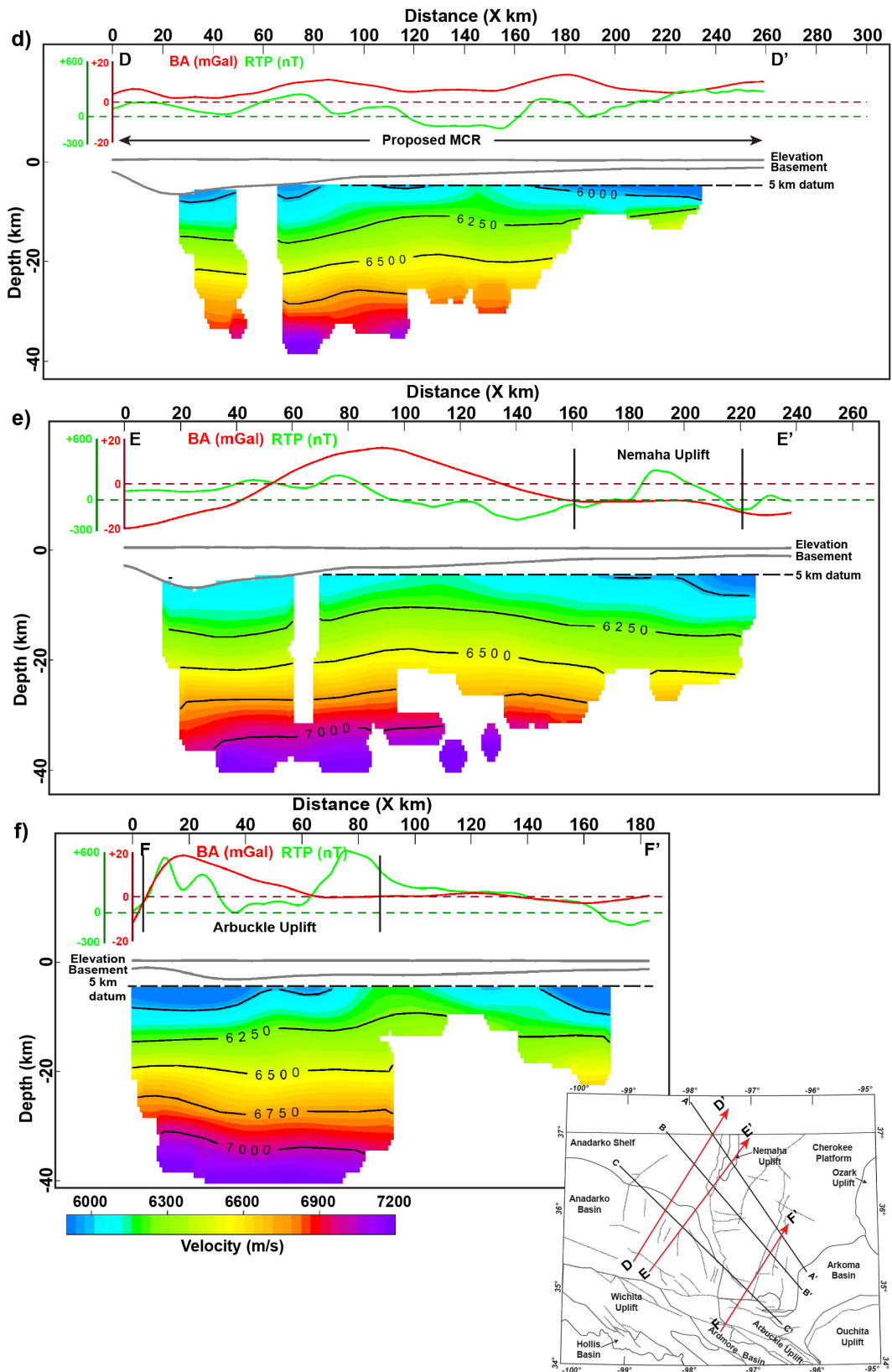


**Figure 10.** Pg-velocity model cross-sections. "Proposed MCR" indicates the tentative continuation of the Midcontinent Rift as suggested by previous studies. See text for discussion.

473 crust. The magnetic high on the southern side (Figure 10f) is close to the Arbuckle up-  
474 lift, which could indicate that this magnetic anomaly is related to the deformation of the  
475 crustal rocks during the uplift. However, we also note is that this area has larger cell size  
476 and comparatively lower number of rays (Figure 5). Subsequently, the velocities here are  
477 less well constrained compared to other parts in our model. The high velocity anomaly  
478 on the northern side in the middle crust is overlain by a low velocity anomaly in the up-  
479 per crust (Figure 10a), which can explain the absence of a gravity anomaly that would be  
480 expected with an isolated high or low velocity anomaly. As gravity data represent the in-  
481 tegrated crustal structure in the subsurface, the combination of this low and high velocity  
482 anomaly may lead to an absence of a pronounced gravity anomaly.

483 We observe lower velocities in the north-east corner (Figure 9b-e; region C) in the  
484 velocity-depth cross-sections up to depths of ~25 km. These low velocity anomalies can  
485 be correlated with the Nemaha uplift in this area. The low velocity anomaly seems to ex-  
486 tend deeper than 25 km into the lower crust (Figure 9f) but due to lack of data coverage  
487 in region C deeper than 30 km, it is difficult to estimate the depth extent of this anomaly.  
488 AA' and EE' (Figure 10) show a decrease in mid-crustal P-wave velocity associated with  
489 the Nemaha uplift and northern part of the Nehama fault system in cross sections that run  
490 both across and along this fault zone. The lower velocities are observed up to 25 – 30  
491 km depth, which suggests that the Nemaha fault zone has a deep root in the crust. The  
492 Wilzetta fault zone is also observed as a low velocity anomaly in the upper crust in the  
493 AA' cross-section. The Anadarko basin region in the west is represented with generally  
494 lower velocities in the upper, mid, and lower crust (Figure 9).

495 P-wave velocities in the lower crust range from 7-7.3 km/s which are higher than the  
496 global average for shields and platform tectonic regime (Christensen & Mooney, 1995).  
497 Our velocity model therefore is in agreement with the assumption of a mafic lower crust  
498 in Oklahoma, as suggested by several crustal evolution models. High lower crustal veloc-  
499 ities were also observed in the vintage 2-D active seismic survey in Oklahoma (Brewer &  
500 Oliver, 1980; Buckey, 2012; Mitchell & Landisman, 1970; Tryggvason & Qualls, 1967).  
501 The presence of a high velocity lower crust throughout Oklahoma provides a strong evi-  
502 dence for the formation of granite-rhyolite province through crustal melting of older crust.  
503 Velocities in the lower crust as seen in BB', DD' and EE' (Figure 10) are mostly homo-  
504 geneous and do not show significant lateral variations. We do not observe variation across  
505 the “Nd-line” in Oklahoma either. The “Nd-line” is regarded as a “suture-zone” based on

506 model age studies of the mid-continent's basement rocks (Nelson & DePaolo, 1985). Lack  
507 of velocity variations across the assumed suture zone does not confirm or deny its exist-  
508 tence, as episodic accretion could have created a more complex terrain with the possibility  
509 of several sutures over time. Also, a variation in age does not necessarily imply a strong  
510 variation of velocity.

### 511 **4.3 Implications on the Midcontinent Rift (MCR) Structure**

512 The MCR, which is extended to central Kansas by most authors (Cannon & Hinze,  
513 1992; Van Schmus & Hinze, 1985; Woelk & Hinze, 1991) (Figure 1), has a thick igneous  
514 crust formed as a result of syn-rift and post-rift igneous fill followed by basin inversion  
515 which thickened the crust further (C. A. Stein et al., 2015). The rift was formed about  
516 1.1 Ga through extensional tectonics related to the collision of Laurentia and Amazonia  
517 and volcanism that is attributed to the presence of the mantle plume in the lithosphere  
518 (Van Schmus & Hinze, 1985; Vervoort & Green, 1997). The rift underwent compressive  
519 inversion which led to the thickening of the crust (C. A. Stein et al., 2015). In general,  
520 rifts are associated with low gravity anomalies due to the accommodation space created  
521 by the rift being filled by sedimentary rocks which have lower densities (C. A. Stein et al.,  
522 2015; S. Stein et al., 2018). The MCR is very unique in that the rift is filled with volumi-  
523 nous basalts and volcanic sequences that give it the characteristic strong positive gravity  
524 anomalies.

525 There is no clear evidence for surface and/or subsurface structural expression of  
526 the MCR in Oklahoma so far. Positive gravity anomalies in northern Oklahoma (Figure  
527 1) have been used to postulate the existence of the MCR in Oklahoma (Kolawole et al.,  
528 2020; C. A. Stein et al., 2014) but the actual magnitudes of these anomalies are smaller  
529 by factors of 3 to 15 compared to the MCR in Kansas and Minnesota. Our model shows  
530 that positive but still moderate velocity anomalies can be associated with the gravity highs  
531 in the upper crust (~5-20 km). As discussed before, these anomalies are interpreted as in-  
532 trusive sills in the basement. These high-velocity anomalies do not extend deeper which  
533 questions the presence of a rift structure in northern Oklahoma. Cross section CC' (Fig-  
534 ure 10) show velocity variations across the proposed MCR. The high  $V_p$  anomaly associ-  
535 ated with the gravity high is more prominent in the upper crust-middle crust in this cross-  
536 section. EE' cross-section cuts through the same gravity high as CC' but in an orientation  
537 parallel to the proposed rift structure (Figure 10). It is more evident in the profile EE' that

538 the velocity anomaly associated with the gravity high is related to the structure of the up-  
539 per crust. DD' cross-section runs along the longitudinal axis of the proposed MCR. The  
540 lateral variation in P-wave velocity in the upper crust (lower velocities in the south and  
541 comparatively high velocities in the north) can also be correlated with the basement below  
542 the Anadarko basin structure which exhibits overall lower crustal velocities.

543 The geology of the mid-continent region has been influenced by several tectonic  
544 events, starting from the episodic emplacement of the granite-rhyolite province from 1.5-  
545 1.3 Ga, followed by midcontinent rifting event 1.1 Ga, Grenville orogeny (1.3-1.09 Ga)  
546 which led to the final assembly of Rodinia, followed by the intermittent breakup of Ro-  
547 dinia which lasted from 0.78-0.53 Ga, and finally led to the formation of the Southern  
548 Oklahoma Aulacogen. Mafic intrusions in the crust upper-middle crust which are related  
549 to the high velocity anomaly are present not only in the proposed MCR region but are  
550 also observed in several active seismic studies in Oklahoma and elsewhere in the granite-  
551 rhyolite terrain in the Southern Oklahoma Aulacogen, Osage county, and northwest Texas  
552 (Buckey, 2012; Brewer et al., 1981, 1983, 1984; Elebiju et al., 2011; Mitchell & Landis-  
553 man, 1970; McBride et al., 2018). We also interpret similar intrusive structures in the  
554 "Region B" in our velocity model as high velocity anomaly. The widespread presence  
555 of such structures across the southern granite-rhyolite terrain, suggests that the intrusions  
556 could be a result of a large-scale tectonic episode, and not necessarily related to the MCR.

#### 557 **4.4 Seismic Velocities and Spatial Distribution of Seismicity**

558 The spatio-temporal distribution of seismicity in the investigated area is related to  
559 factors such as the presence of injection wells, injection volume, optimal fault orientations,  
560 porosity and permeability, and basement rock lithology (Ellsworth, 2013; Keranen et al.,  
561 2014; Qin et al., 2018, 2019). Many of the earthquakes in Oklahoma have occurred on  
562 previously unmapped faults, thus a lack of mapped faults cannot be used to argue for the  
563 lack of seismicity in this area. Figure 11 illustrates the location of earthquakes, injection  
564 wells, and injection volumes in the area. We have considered only the wells classified as  
565 salt-water disposal wells for this analysis, as the seismicity in Oklahoma has been con-  
566 nected to the waste water injection wells (Keranen et al., 2014). We observe a pronounced  
567 lack of seismicity in the high-velocity region A (Figure 11). In this area, the number of  
568 injection wells is still significant, and the injection volumes are similar to areas with high  
569 seismicity. We therefore argue that the lack of earthquakes in this area is related to the

570 variable basement lithology as indicated by the velocity distribution. Lithologic control on  
 571 seismicity is observed in eastern Oklahoma, where high-volume injection wells have not  
 572 caused an increase in seismicity (Shah & Keller, 2017). We suggest that the rocks asso-  
 573 ciated with the high velocity anomalies are likely to have higher rock strength and thus  
 574 would require higher stress conditions for fault rupture, and /or this basement region hosts  
 575 less faults. This high velocity anomaly in shallow depths might be minimally fractured as  
 576 compared to surrounding regions. Minimal fracturing would also imply low permeabil-  
 577 ity and less vertical fluid migration, which would eventually lead to comparably low pore  
 578 pressure buildup in the region. Basement lithology can influence the pore space availabil-  
 579 ity, permeability and deformation capability, all of which in turn could control seismicity.  
 580 As discussed above, deeper velocity anomalies in this region are also related to mafic in-  
 581 trusions at larger depths, and the anomaly is further confined by the Nemaha fault system  
 582 to the east, as are the earthquake locations. We argue that all these observations suggest  
 583 that the Nemaha fault system is a deep-rooted crustal boundary with separates two crustal  
 584 domains of different origin.

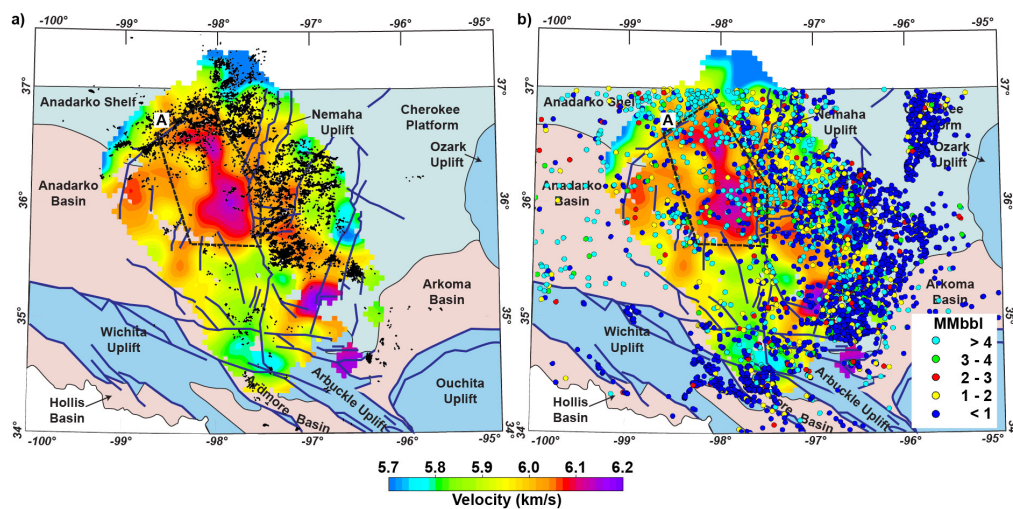


**Figure 11.** a) Earthquake locations; b) Total injection volume (MMbbl) for saltwater disposal wells from 2011-2017, overlain on 5 km velocity-depth slice.

## 585 5 Conclusions

586 In this study, common-mid-point sorting, stacking, and inversion techniques are ap-  
 587 plied to local earthquake waveform data in the central part of the mid-continent. In con-

588 trast to traditional local earthquake tomography (LET) studies from Oklahoma that have  
589 imaged the upper crust, our methodology results in a 3-D velocity model for significantly  
590 larger depths. Our results suggest a more heterogeneous upper and middle crust and a rel-  
591 atively homogeneous lower crust. These observations are interpreted to reflect a complex  
592 geologic history including deformations in the upper and mid-crustal depths and a possi-  
593 ble homogenization of the lower crust through melting. The high velocity ( $>7$  km/s) lower  
594 crust is indicative of mafic composition. This provides strong evidence for the evolution  
595 of the Granite-Rhyolite province from basaltic underplating and crustal melting. Structural  
596 evidence for a deep Midcontinent rift structure is not observed in Oklahoma. Several (pos-  
597 sibly mafic) intrusions are interpreted in the upper-middle crust from high velocity anoma-  
598 lies which have previously been associated to the MCR extension in Oklahoma. However,  
599 the widespread occurrence of these intrusions in Oklahoma may suggest their derivation  
600 from a regional tectonic event as opposed to more local MCR event in Oklahoma. We in-  
601 terpret the Nemaha fault system as a deep-seated discontinuity which separates two crustal  
602 domains of different origin. Our results also suggest a lithologic control on induced seis-  
603 micity in Oklahoma.

604 The suggested workflow is potentially applicable to other areas with similar datasets.  
605 Robust 3-D velocity models derived by this methodology can also be used for improved  
606 earthquake localization, and as initial models for local high-resolution LET analysis.

### 607 **Acknowledgments**

608 Waveform data used in this study can be downloaded from Incorporated Research Institu-  
609 tions for Seismology Data Management Center (IRIS-DMC, <https://ds.iris.edu/ds/nodes/dmc/data/#access>). Earthquake catalog for Oklahoma can be accessed through  
610 Oklahoma Geological Survey at [http://www.ou.edu/ogs/research/earthquakes/](http://www.ou.edu/ogs/research/earthquakes/catalogs)  
611 [catalogs](http://www.ou.edu/ogs/research/earthquakes/catalogs). We would like to thank Dr. Brett Carpenter and Dr. Xiaowei Chen for thought-  
612 ful discussions that greatly improved our manuscript. We would also like to thank Dr. Jef-  
613 ferson Chang for providing the HypoDD relocated catalog used in this study.  
614

### 615 **References**

616 Agena, W. F., Lee, M. W., & Grow, J. A. (1989). *Reprocessing of the COCORP data*  
617 *recorded across the Wichita Mountain uplift and the Anadarko basin in southern Okla-*  
618 *homa* (Tech. Rep.).

- 619 Amato, J. M., Heizler, M. T., Boullion, A. O., Sanders, A. E., Toro, J., McLemore, V. T.,  
 620 & Andronicos, C. L. (2011). Syntectonic 1.46 Ga magmatism and rapid cooling of  
 621 a gneiss dome in the southern Mazatzal Province: Burro Mountains, New Mexico.  
 622 *Geological Society of America Bulletin*, 123(9-10), 1720–1744. doi: 10.1130/B30337  
 623 .1
- 624 Anderson, J., & Bender, E. (1989). Nature and origin of Proterozoic A-type granitic mag-  
 625 matism in the southwestern United States of America. *Lithos*, 23(1-2), 19–52. doi:  
 626 10.1016/0024-4937(89)90021-2
- 627 Astiz, L., Earle, P., & Shearer, P. (1996). Global Stacking of Broadband Seismograms.  
 628 *Seismological Research Letters*, 67(4), 8–18. doi: 10.1785/gssrl.67.4.8
- 629 Behm, M. (2009). 3-D modelling of the crustal S -wave velocity structure from active source  
 630 data: application to the Eastern Alps and the Bohemian Massif. *Geophysical Journal*  
 631 *International*, 179(1), 265–278. doi: 10.1111/j.1365-246X.2009.04259.x
- 632 Behm, M., Brückl, E., Chwatal, W., & Thybo, H. (2007). Application of stacking and in-  
 633 version techniques to three-dimensional wide-angle reflection and refraction seismic  
 634 data of the Eastern Alps. *Geophysical Journal International*, 170(1), 275–298. doi:  
 635 10.1111/j.1365-246X.2007.03393.x
- 636 Bickford, M. E., Harrower, K. L., Hoppe, W. J., Nelson, B. K., Nusbaum, R. L., & Thomas,  
 637 J. J. (1981). Rb-Sr and U-Pb geochronology and distribution of rock types in the Pre-  
 638 cambrian basement of Missouri and Kansas. *Geological Society of America Bulletin*,  
 639 92, 323–341. doi: 10.1130/0016-7606(1981)92<323:RAUGAD>2.0.CO;2
- 640 Bickford, M. E., & Lewis, R. D. (1979). U-Pb geochronology of exposed basement rocks  
 641 in Oklahoma. *Geological Society of America Bulletin*, 90(6), 540. doi: 10.1130/0016  
 642 -7606(1979)90<540:UGOEBR>2.0.CO;2
- 643 Bickford, M. E., Van Schmus, W., Karlstrom, K., Mueller, P., & Kamenov, G. (2015).  
 644 Mesoproterozoic-trans-Laurentian magmatism: A synthesis of continent-wide age  
 645 distributions, new SIMS U–Pb ages, zircon saturation temperatures, and Hf and  
 646 Nd isotopic compositions. *Precambrian Research*, 265, 286–312. doi: 10.1016/  
 647 j.precamres.2014.11.024
- 648 Bickford, M. E., Van Schmus, W. R., & Zietz, I. (1986). Proterozoic history of the midcon-  
 649 tinent region of North America. *Geology*, 14(6), 492. doi: 10.1130/0091-7613(1986)  
 650 14<492:PHOTMR>2.0.CO;2
- 651 Braeuer, B., Asch, G., Hofstetter, R., Haberland, C., Jaser, D., El-Kelani, R., & Weber, M.

- 652 (2012). High-resolution local earthquake tomography of the southern Dead Sea area.  
 653 *Geophysical Journal International*, 191(3), 881-897. doi: 10.1111/j.1365-246X.2012  
 654 .05668.x
- 655 Brewer, J. A., Brown, L. D., Steiner, D., Oliver, J. E., Kaufman, S., & Denison, R. E.  
 656 (1981). Proterozoic basin in the southern Midcontinent of the United States re-  
 657 vealed by COCORP deep seismic reflection profiling. *Geology*, 9(12), 569. doi:  
 658 10.1130/0091-7613(1981)9<569:PBITSM>2.0.CO;2
- 659 Brewer, J. A., Good, R., Oliver, J. E., Brown, L. D., & Kaufman, S. (1983). COCORP  
 660 profiling across the Southern Oklahoma aulacogen: Overthrusting of the Wichita  
 661 Mountains and compression within the Anadarko Basin. *Geology*, 11(2), 109. doi:  
 662 10.1130/0091-7613(1983)11<109:CPATSO>2.0.CO;2
- 663 Brewer, J. A., Good, R., Oliver, J. E., Brown, L. D., & Kaufman, S. (1984). COCORP deep  
 664 seismic reflection traverse across the southern Oklahoma Aulacogen. *Technical Pro-  
 665 ceedings of the 1981 AAPG Mid-Continent Regional Meeting, 1984*, 191–194.
- 666 Brewer, J. A., & Oliver, J. E. (1980). Seismic reflection studies of deep crustal structure.  
 667 *Annual Review of Earth and Planetary Sciences*, 8(205-230).
- 668 Buckley, A. (2012). An integrated geophysical analysis of crustal structure in the Wichita  
 669 Uplift region of southern Oklahoma. *The Shale Shaker*, 62(6), 432–452.
- 670 Buehler, J. S., & Shearer, P. M. (2013). Sn propagation in the Western United States from  
 671 common midpoint stacks of USArray data. *Geophysical Research Letters*, 40(23),  
 672 6106–6111. doi: 10.1002/2013GL057680
- 673 Campbell, J. A. (2007). Understanding the structure of the Wichita uplift, southern Okla-  
 674 homa. *Shale Shaker*, 1918(December), 87–97.
- 675 Campbell, J. A., & Weber, J. L. (2006). Wells drilled to basement to basement in Oklahoma.  
 676 *Oklahoma Geological Survey Special Publication 2006-1*.
- 677 Cannon, W. F., & Hinze, W. J. (1992). Speculations on the origin of the North American  
 678 Midcontinent rift. *Tectonophysics*, 213(1-2), 49–55. doi: 10.1016/0040-1951(92)  
 679 90251-Z
- 680 Chen, C. (2016). *Comprehensive analysis of Oklahoma earthquakes: from earthquake  
 681 monitoring to 3D tomography and relocation* (Unpublished doctoral dissertation). Uni-  
 682 versity of Oklahoma.
- 683 Chichester, B., Rychert, C., Harmon, N., Lee, S., Frederiksen, A., & Zhang, H. (2018).  
 684 Seismic Imaging of the North American Midcontinent Rift Using S -to- P Receiver

- 685 Functions. *Journal of Geophysical Research: Solid Earth*, 123(9), 7791–7805. doi:  
 686 10.1029/2018JB015771
- 687 Chopra, S., Marfurt, K. J., Kolawole, F., & Carpenter, B. M. (2018). Nemaha Strike-Slip  
 688 Fault Expression on 3-D Seismic Data in SCOOP Trend. *AAPG Explorer*(June), 18–  
 689 19.
- 690 Christensen, N. I., & Mooney, W. D. (1995). Seismic velocity structure and composition  
 691 of the continental crust: A global view. *Journal of Geophysical Research*, 100(B6),  
 692 9761–9788. doi: 10.1029/95JB00259
- 693 Darold, A. P., Holland, A. A., Jennifer, K., & Gibson, A. R. (2015). *Oklahoma Earthquake*  
 694 *Summary Report 2014* (Tech. Rep.).
- 695 Denison, R. E., Lidiak, E. G., Bickford, M. E., & Kisvarsanyi, E. B. (1984). Geology  
 696 and geochronology of Precambrian rocks in the Central Interior region of the United  
 697 States. *US Geological Survey Professional Paper*, 1241 C, 1–13. doi: 10.3133/  
 698 pp1241c
- 699 Elebiju, O. O., Matson, S., Randy Keller, G., & Marfurt, K. J. (2011). Integrated geophysical  
 700 studies of the basement structures, the Mississippi chert, and the Arbuckle Group of  
 701 Osage County region, Oklahoma. *AAPG Bulletin*, 95(3), 371–393. doi: 10.1306/  
 702 08241009154
- 703 Ellsworth, W. L. (2013). Injection-Induced Earthquakes. *Science*, 341(6142), 1225942–  
 704 1225942. doi: 10.1126/science.1225942
- 705 Evanzia, D., Pulliam, J., Ainsworth, R., Gurrola, H., & Pratt, K. (2014). Seismic Vp & Vs  
 706 tomography of Texas & Oklahoma with a focus on the Gulf Coast margin. *Earth and*  
 707 *Planetary Science Letters*, 402(C), 148–156. doi: 10.1016/j.epsl.2013.12.027
- 708 Frost, C. D., & Frost, B. R. (2011). On Ferroan (A-type) Granitoids: their Compositional  
 709 Variability and Modes of Origin. *Journal of Petrology*, 52(1), 39–53. doi: 10.1093/  
 710 petrology/egq070
- 711 Frost, C. D., & Frost, B. R. (2013). Proterozoic ferroan feldspathic magmatism. *Precam-*  
 712 *brian Research*, 228, 151–163. doi: 10.1016/j.precamres.2013.01.016
- 713 Gajewski, D., & Pšenčík, I. (1987). Computation of high-frequency seismic wavefields in  
 714 3-D laterally inhomogeneous anisotropic media. *Geophysical Journal International*,  
 715 91(2), 383–411. doi: 10.1111/j.1365-246X.1987.tb05234.x
- 716 Gajewski, D., & Pšenčík, I. (1989). Ray synthetic seismograms in 3-d laterally inhomoge-  
 717 neous anisotropic structures-program anray89. *LBL Center for Computational Seis-*

- 718 *mology, Berkeley, CA.*
- 719 Garner, D. L., & Turcotte, D. L. (1984). The thermal and mechanical evolution of the  
720 Anadarko basin. *Tectonophysics*, 107(1-2), 1–24. doi: 10.1016/0040-1951(84)90026  
721 -X
- 722 Gilbert, M., Denison, R., Reed, J., Bickford, M., Houston, R., Link, P., . . . Van Schmus, W.  
723 (1993). Late proterozoic to early cambrian basement of oklahoma. *Reed JC, Bickford*  
724 *ME, Houston RS, and four others, eds., Precambrian: Conterminous US: Boulder,*  
725 *Colorado, Geological Society of America, The Geology of North America, 2, 303–*  
726 *314.*
- 727 Goodge, J. W., & Vervoort, J. D. (2006). Origin of Mesoproterozoic A-type granites in  
728 Laurentia: Hf isotope evidence. *Earth and Planetary Science Letters*, 243(3-4), 711–  
729 731. doi: 10.1016/j.epsl.2006.01.040
- 730 Hinze, W. J., Allen, D. J., Braile, L. W., & Mariano, J. (1997). The Midcontinent Rift Sys-  
731 tem: A major Proterozoic continental rift. In *Middle proterozoic to cambrian rifting,*  
732 *central north america* (Vol. 312, pp. 7–35). Geological Society of America. doi:  
733 10.1130/0-8137-2312-4.7
- 734 Johnson, K. (2008). Geologic History of Oklahoma. *Educational Publication*, 9, 3–8.
- 735 Karlstrom, K. E., Whitmeyer, S. J., Dueker, K., Williams, M. L., Bowring, S. A., Levander,  
736 A. R., . . . Keller, G. R. (2005). Synthesis of results from the CD-ROM Experiment:  
737 4-D image of the lithosphere beneath the Rocky Mountains and implications for under-  
738 standing the evolution of continental lithosphere. In *Geophysical monograph series*  
739 (Vol. 154, pp. 421–441). doi: 10.1029/154GM31
- 740 Karlstrom, K. E., Åhäll, K.-I., Harlan, S. S., Williams, M. L., McLelland, J., & Geissman,  
741 J. W. (2001). Long-lived (1.8–1.0 ga) convergent orogen in southern laurentia, its  
742 extensions to australia and baltica, and implications for refining rodinia. *Precambrian*  
743 *Research*, 111(1), 5 - 30. doi: [https://doi.org/10.1016/S0301-9268\(01\)00154-1](https://doi.org/10.1016/S0301-9268(01)00154-1)
- 744 Keller, G., Lidiak, E., Hinze, W., & Braile, L. (1983). The Role of Rifting in the Tectonic  
745 Development of the Midcontinent, U.S.A. In *Tectonophysics* (Vol. 94, pp. 391–412).  
746 doi: 10.1016/B978-0-444-42198-2.50028-6
- 747 Keranen, K. M., Weingarten, M., Abers, G. A., Bekins, B. A., & Ge, S. (2014). Sharp in-  
748 crease in central Oklahoma seismicity since 2008 induced by massive wastewater in-  
749 jection. *Science*, 345(6195), 448–451. doi: 10.1126/science.1255802
- 750 Kissling, E., Ellsworth, W. L., Eberhart-Phillips, D., & Kradolfer, U. (1994). Initial refer-

- 751           ence models in local earthquake tomography. *Journal of Geophysical Research: Solid*  
752           *Earth*, 99(B10), 19635–19646. doi: 10.1029/93JB03138
- 753   Kolawole, F., Simpson Turko, M., & Carpenter, B. M. (2020). Basement-controlled defor-  
754           mation of sedimentary sequences, Anadarko Shelf, Oklahoma. *Basin Research*(August  
755           2019), bre.12433. doi: 10.1111/bre.12433
- 756   Lidiak, E. G. (1996). Geochemistry of subsurface Proterozoic rocks in the eastern Mid-  
757           continent of the United States: Further evidence for a within-plate tectonic setting. In  
758           *Basement and basins of eastern north america* (Vol. 308, pp. 45–66). Geological Soci-  
759           ety of America. doi: 10.1130/0-8137-2308-6.45
- 760   Loidl, B., Behm, M., Thybo, H., & Stratford, W. (2014). Three-dimensional seismic model  
761           of crustal structure in Southern Norway. *Geophysical Journal International*, 196(3),  
762           1643–1656. doi: 10.1093/gji/ggt471
- 763   Lynn, H. B., Hale, L. D., & Thompson, G. A. (1981). Seismic reflections from the basal con-  
764           tacts of batholiths. *Journal of Geophysical Research: Solid Earth*, 86(B11), 10633–  
765           10638. doi: 10.1029/JB086iB11p10633
- 766   McBride, J. H., William Keach, R., Leetaru, H. E., & Smith, K. M. (2018). Visualizing  
767           Precambrian basement tectonics beneath a carbon capture and storage site, Illinois  
768           Basin. *Interpretation*, 6(2), T257-T270. doi: 10.1190/INT-2017-0116.1
- 769   McGlannan, A. J., & Gilbert, H. (2016). Crustal signatures of the tectonic development of  
770           the North American midcontinent. *Earth and Planetary Science Letters*, 433, 339–  
771           349. doi: 10.1016/j.epsl.2015.10.048
- 772   Mitchell, B., & Landisman, M. (1970). Interpretation of a crustal section across Oklahoma.  
773           *Geological Society of America Bulletin*, 81, 2647–2656.
- 774   Muehlberger, W. R., Denison, R. E., & Lidiak, E. G. (1967). Basement Rocks in Continental  
775           Interior of United States. *AAPG Bulletin*, 51(12), 2351–2380. doi: 10.1306/5D25C277  
776           -16C1-11D7-8645000102C1865D
- 777   Muehlberger, W. R., Hedge, C. E., Denison, R. E., & Marvin, R. F. (1966). Geochronology  
778           of the midcontinent region, United States: 3. Southern area. *Journal of Geophysical*  
779           *Research*, 71(22), 5409–5426. doi: 10.1029/JZ071i022p05409
- 780   Nelson, B. K., & DePaolo, D. J. (1985). Rapid production of continental crust 1.7 to 1.9 b.y.  
781           ago: Nd isotopic evidence from the basement of the North American mid-continent.  
782           *Geological Society of America Bulletin*, 96(6), 746. doi: 10.1130/0016-7606(1985)  
783           96<746:RPOCCT>2.0.CO;2

- 784 Northcutt, R. A., & Campbell, J. A. (1996). Geologic Provinces of Oklahoma. *Shale Shaker*.  
785 doi: 10.1306/7834D65C-1721-11D7-8645000102C1865D
- 786 Pei, S., Chen, Y. J., Feng, B., Gao, X., & Su, J. (2013). High-resolution seismic ve-  
787 locity structure and azimuthal anisotropy around the 2010 Ms=7.1 Yushu earth-  
788 quake, Qinghai, China from 2D tomography. *Tectonophysics*, 584, 144–151. doi:  
789 10.1016/j.tecto.2012.08.020
- 790 Pei, S., Peng, Z., & Chen, X. (2018). Locations of Injection-Induced Earthquakes in Okla-  
791 homa Controlled by Crustal Structures. *Journal of Geophysical Research: Solid Earth*,  
792 123(3), 2332–2344. doi: 10.1002/2017JB014983
- 793 Phinney, R. A., & Jurdy, D. M. (1979). Seismic imaging of deep crust. *Geophysics*, 44(10),  
794 1637–1660. doi: 10.1190/1.1440927
- 795 Pratt, T. L., Hauser, E. C., & Nelson, K. D. (1992). Widespread buried precambrian lay-  
796 ered sequences in the midcontinent- evidence for large proterozoic depositional basins.  
797 *AAPG Bulletin*, 76(9), 1384–1401.
- 798 Qin, Y., Chen, X., Carpenter, B. M., & Kolawole, F. (2018). Coulomb Stress Transfer In-  
799 fluences Fault Reactivation in Areas of Wastewater Injection. *Geophysical Research*  
800 *Letters*, 45(20), 059–11. doi: 10.1029/2018GL079713
- 801 Qin, Y., Chen, X., Walter, J. I., Haffener, J., Trugman, D. T., Carpenter, B. M., . . . Kolawole,  
802 F. (2019). Deciphering the Stress State of Seismogenic Faults in Oklahoma and South-  
803 ern Kansas Based on an Improved Stress Map. *Journal of Geophysical Research:*  
804 *Solid Earth*, 124(12), 12920–12934. doi: 10.1029/2019JB018377
- 805 Rawlinson, N., & Sambridge, M. (2003). Seismic traveltime tomography of the crust and  
806 lithosphere. In *Advances in geophysics* (Vol. 46, pp. 81–198). doi: 10.1016/S0065  
807 -2687(03)46002-0
- 808 Schoenball, M., & Ellsworth, W. L. (2017). Waveform-Relocated Earthquake Catalog for  
809 Oklahoma and Southern Kansas Illuminates the Regional Fault Network. *Seismologi-*  
810 *cal Research Letters*, 88(5), 1252–1258. doi: 10.1785/0220170083
- 811 Shah, A. K., & Keller, G. R. (2017). Geologic influence on induced seismicity: Constraints  
812 from potential field data in Oklahoma. *Geophysical Research Letters*, 44(1), 152–161.  
813 doi: 10.1002/2016GL071808
- 814 Shaw, C. A., Heizler, M. T., & Karlstrom, K. E. (2005). <sup>40</sup>Ar/<sup>39</sup>Ar thermochronologic  
815 record of 1.45–1.35 Ga intracontinental tectonism in the southern Rocky Mountains:  
816 Interplay of conductive and advective heating with intracontinental deformation. In

- 817 *Geophysical monograph series* (Vol. 154, pp. 163–184). doi: 10.1029/154GM12
- 818 Shen, W., Ritzwoller, M. H., & Schulte-Pelkum, V. (2013). Crustal and uppermost mantle  
819 structure in the central U.S. encompassing the Midcontinent Rift. *Journal of Geophys-*  
820 *ical Research: Solid Earth*, 118(8), 4325–4344. doi: 10.1002/jgrb.50321
- 821 Sims, P. K., Saltus, R. W., & Anderson, E. D. (2005). Structure Map of the Continental  
822 United States – An Interpretation of Geologic and Aeromagnetic Data of the Conti-  
823 nental United States — an Interpretation of Geologic and Aeromagnetic Data. *U.S.*  
824 *Geological Survey Open-file report 2005-1029*, 29.
- 825 Slagstad, T., Culshaw, N. G., Daly, J. S., & Jamieson, R. A. (2009). Western Grenville  
826 Province holds key to midcontinental Granite-Rhyolite Province enigma. *Terra Nova*,  
827 21(3), 181–187. doi: 10.1111/j.1365-3121.2009.00871.x
- 828 Stein, C. A., Kley, J., Stein, S., Hindle, D., & Keller, G. R. (2015). North America’s Mid-  
829 continent Rift: When rift met LIP. *Geosphere*, 11(5), 1607–1616. doi: 10.1130/  
830 GES01183.1
- 831 Stein, C. A., Stein, S., Elling, R., Keller, G. R., & Kley, J. (2018). Is the “Grenville Front” in  
832 the central United States really the Midcontinent Rift? *GSA Today*, 28(5), 4–10. doi:  
833 10.1130/GSATG357A.1
- 834 Stein, C. A., Stein, S., Merino, M., Randy Keller, G., Flesch, L. M., & Jurdy, D. M. (2014).  
835 Was the Midcontinent Rift part of a successful seafloor-spreading episode? *Geophysi-*  
836 *cal Research Letters*, 41(5), 1465–1470. doi: 10.1002/2013GL059176
- 837 Stein, S., Stein, C. A., Elling, R., Kley, J., Keller, G. R., Wysession, M., . . . Moucha, R.  
838 (2018). Insights from north america’s failed midcontinent rift into the evolution of  
839 continental rifts and passive continental margins. *Tectonophysics*, 744, 403–421.
- 840 Tave, M. A. (2013). *Imaging of the crust and moho beneath oklahoma using receiver func-*  
841 *tions and pn tomography; with emphasis on the southern oklahoma aulacogen* (Unpub-  
842 lished doctoral dissertation).
- 843 Thomas, W. A. (1991). The appalachian-ouachita rifted margin of southeastern north amer-  
844 ica. *Geological Society of America Bulletin*, 103(3), 415–431.
- 845 Thybo, H., & Artemieva, I. (2013). Moho and magmatic underplating in continental litho-  
846 sphere. *Tectonophysics*, 609, 605–619. doi: 10.1016/j.tecto.2013.05.032
- 847 Thybo, H., Sandrin, A., Nielsen, L., Lykke-Andersen, H., & Keller, G. (2006). Seismic ve-  
848 locity structure of a large mafic intrusion in the crust of central Denmark from project  
849 ESTRID. *Tectonophysics*, 420(1-2), 105–122. doi: 10.1016/j.tecto.2006.01.029

- 850 Tong, P., Yang, D., Li, D., & Liu, Q. (2017). Time-evolving seismic tomography: The  
 851 method and its application to the 1989 loma prieta and 2014 south napa earthquake  
 852 area, california. *Geophysical Research Letters*, *44*(7), 3165–3175.
- 853 Toth, C. R. (2014). *Separation of the earthquake tomography inverse problem to refine*  
 854 *hypocenter locations and tomographic models: A case study from central oklahoma*  
 855 (Unpublished doctoral dissertation). University of Oklahoma.
- 856 Tryggvason, E., & Qualls, B. R. (1967). Seismic refraction measurements of crustal structure  
 857 in Oklahoma. *Journal of Geophysical Research*, *72*(14), 3738–3740. doi: 10.1029/  
 858 JZ072i014p03738
- 859 Van Schmus, W. R., Bickford, M. E., & Turek, A. (1996). Proterozoic geology of the east-  
 860 central Midcontinent basement. In *Basement and basins of eastern north america*  
 861 (Vol. 308, pp. 7–32). Geological Society of America. doi: 10.1130/0-8137-2308-6.7
- 862 Van Schmus, W. R., & Hinze, W. J. (1985). The Midcontinent Rift System. *Annual Review*  
 863 *of Earth and Planetary Sciences*, *13*(1), 345–383. doi: 10.1146/annurev.ea.13.050185  
 864 .002021
- 865 Vervoort, J. D., & Green, J. C. (1997). Origin of evolved magmas in the Midcontinent  
 866 rift system, northeast Minnesota: Nd-isotope evidence for melting of Archean crust.  
 867 *Canadian Journal of Earth Sciences*, *34*(4), 521–535. doi: 10.1139/e17-042
- 868 Whitmeyer, S. J., & Karlstrom, K. E. (2007). Tectonic model for the Proterozoic growth of  
 869 North America. *Geosphere*, *3*(4), 220–259. doi: 10.1130/GES00055.1
- 870 Woelk, T. S., & Hinze, W. J. (1991). Model of the midcontinent rift system in northeastern  
 871 Kansas. *Geology*, *19*(3), 277. doi: 10.1130/0091-7613(1991)019<0277:MOTMRS>2  
 872 .3.CO;2
- 873 Zhang, H., Lee, S., Wolin, E., Bollmann, T. A., Revenaugh, J., Wiens, D. A., . . . Jurdy,  
 874 D. M. (2016). Distinct crustal structure of the North American Midcontinent Rift from  
 875 P wave receiver functions. *Journal of Geophysical Research: Solid Earth*, *121*(11),  
 876 8136–8153. doi: 10.1002/2016JB013244
- 877 Zhu, X., & McMechan, G. A. (1989). 2-D tomographic imaging of velocities in the Wichita  
 878 uplift-Anadarko basin region of southwestern Oklahoma. *Bulletin of the Seismological*  
 879 *Society of America*, *79*(3), 873–887.